USING MULTIMODAL MRI TECHNIQUES TO UNDERSTAND THE ROLE OF HIPPOCAMPUS IN SCHIZOPHRENIA

APPROVED BY SUPERVISORY COMMITTEE

_____
Carol Tamminga, M.D.
Professor of Psychiatry

_____
Robert Lenkinski, Ph.D.
Professor of Radiology

_____
Changho Choi, Ph.D.
Associate Professor of AIRC

_____
Hanzhang Lu, Ph.D.
Associate Professor of AIRC

_____
Elizabeth Maher, M.D., Ph.D.
Associate Professor of
Internal Medicine

DEDICATION

To my parents, for their everlasting support and love.

USING MULTIMODAL MRI TECHNIQUES TO UNDERSTAND THE ROLE OF HIPPOCAMPUS IN SCHIZOPHRENIA

By

Yan Fang

DISSERTATION

Presented to the Faculty of the Graduate School of Biomedical Sciences

The University of Texas Southwestern Medical Center at Dallas

For the Degree of

DOCTOR OF PHILOSOPHY

Dallas, Texas

August, 2013

ACKNOWLEDGEMENTS

I’m grateful to my advisor Dr. Carol Tamminga for her visionary and patient instructions during my Ph.D. study. I also owe my thanks to my former advisors Dr. Richard Briggs and Dr. Kaundinya Gopinath for teaching me the MRI skills.

I appreciate all my former and current colleagues and our collaborators, especially Dr. Hanzhang Lu, Dr. Changho Choi, Dr. Jinsoo Uh, Binu Thomas, Dr. Carolyn Sacco, Dr. Ana Stan, Dr. Elena Ivleva and Perry Mihalakos. Without their hard work and help, we cannot finish this excellent work.

Finally, without the consistent support from my families and my friends, I will never be able to finish my Ph.D. study. I hope they can share my joy at this moment.

USING MULTIMODAL MRI TECHNIQUES TO UNDERSTAND THE ROLE OF HIPPOCAMPUS IN SCHIZOPHRENIA

Publication No._____

Yan Fang, Ph.D.

The University of Texas Southwestern Medical Center at Dallas, 2013

Supervising Professor: Carol Tamminga, M.D.

ABSTRACT

According to our hippocampal metaplasticity model for schizophrenia (SZ), reduced glutamate signaling in dentate gyrus could lower the LTP threshold in its target region CA3, thus generates increased associative function in CA3, resulting in memories with psychotic content. The loss of mnemonic functions in dentate gyrus could decrease its pattern separation function. Multimodal MRI techniques including proton magnetic resonance spectroscopy (^{1}H-MRS), cerebral blood volume (CBV), cerebral blood flow (CBF) and functional MRI at 3T were used to examine the metaplasticity model and probe the role of hippocampus in schizophrenia both with (SZ-on) and without (SZ-off) antipsychotic drug treatment.

Single-voxel localized scalar (J) difference editing sequence was used in ^{1}H MRS to measure glutamate (Glu), GABA and N-acetylaspartate (NAA) concentrations in the left hippocampus in normal control (NC), SZ-on and SZ-off groups. Significant decreases in Glu and NAA concentrations relative to creatine (Cr) were found in SZ group, which confirms our hypothesis of decreased dentate gyrus glutamatergic output in SZ. High resolution vascular-space occupancy (VASO) technique using Gd-DTPA as contrast agent acquired CBV maps with resolution of 0.78mm x 0.78 mm x 4 mm, and found increased CA3+CA1+Sub relative CBV value normalized by thalamus CBV in SZ group compared to NC group, which suggests a basal hypermetabolic state in these hippocampal subregions in SZ. Pseudo-continuous arterial spin labeling (pCASL) was used to measure whole brain CBF at standard resolution, and we found hippocampal CBF had positive correlation with PANSS total scores. In the acquired equivalence (AE) fMRI study, reduced midbrain and hippocampal activity was found in both trained and transfer tasks in SZ-on group compared to NC group. The behavior data also support this finding although lacking statistical significance, which may indicate a hyperactivity-induced inefficiency in memory processing in hippocampus.

Some of our results support while some modify our original hypotheses. The reduced glutamate concentration in left hippocampus can be interpreted as deriving from the putative NMDA receptor lesion in dentate gyrus in SZ. And that the hypoglutamatergic lesion in dentate gyrus would be sufficient to generate reduced hippocampal glutamate detected by MRS is demonstrated in our NR1-KO mouse study. The increased basal neuronal activity in CA3 and CA1 is supposed to decrease the efficiency of the pattern completion function within CA3, resulting in hyperassociative memory. The positive correlation between hippocampal CBF and PANSS total reveals that the increased CBF in hippocampus is related to psychosis. The AE fMRI result also gives a support to our hypothesis. We could not distinguish the SZ-on and SZ-off groups in our ^{1}H MRS and VASO studies. This might be due to the limited sample sizes of these studies. In the AE fMRI study, the SZ-off group had better performance than the SZ-on group and the brain activity of the SZ-off group was more similar to the NC group compared to the SZ-on group, which contradicts our prediction. The age range and the match between groups shall be considered more strictly in our future studies.

TABLE OF CONTENTS

TITLE FLY……i

DEDICATION……ii

TITLE PAGE……iii

COPYRIGHT………iv

ACKNOWLEDGEMENTS………v

ABSTRACT……vii

TABLE OF CONTENTS……ix

LIST OF FIGURES……xii

LIST OF TABLES……xiv

LIST OF ABBREVIATIONS……xv

CHAPTER ONE: Background……1

Schizophrenia……1

Neuroanatomy basics of schizophrenia……2

Biochemistry background of schizophrenia……4

The dopamine and glutamate hypotheses of schizophrenia……6

Hippocampus and schizophrenia……7

Hippocampal metaplasticity model for schizophrenia……9

CHAPTR TWO: Proton MRS measurement in Hippocampus.....12

Introduction.....12

^{1}H-MRS Method.....13

Research participants.....14

MRI scans.....14

MRS data analysis.....16

Result.....17

Discussion.....19

Future 7T experiment.....21

CHAPTER THREE: CBV and CBF measurements in Hippocampus.....24

A. VASO study.....24

Introduction.....24

High-resolution VASO method.....24

MRI scans.....26

VASO data analysis.....28

Result.....30

Discussion.....31

B. pCASL study.....33

Introduction.....33

MRI scans.....34

pCASL data analysis……..35

Result……..37

Discussion……39

CHAPTER FOUR: Acquired Equivalence (AE) Task measurement using fMRI……40

Introduction……40

Acquired equivalence (AE) task……..42

Experimental method……..43

Data analysis……45

Result……49

Discussion……54

CHAPTER FIVE: Conclusion……57

BIBLIOGRAPHY……59

APPENDICES……73

A. VASO script……73

B. pCASL script……97

C. AE ROI analysis script……101

LIST OF FIGURES

Figure 1. Dopamine Pathways……...…..5

Figure 2. Hippocampal metaplasticity model for schizophrenia……10

Figure 3. ^{1}H-MRS single voxel position……..14

Figure 4. Typical spectrums acquired in this study……..15

Figure 5. Glu, NAA and GABA concentrations in the NC group and SZ group……18

Figure 6. Glutamate correlations with the PANSS total score and PANSS negative score within the SZ group……19

Figure 7. Inversion recovery curves for three proton species with different T_1 values at 1.5 T..25

Figure 8. PANSS positive score distribution and PANSS total score distribution in SZ-on and SZ-off groups in VASO study……26

Figure 9. Timing diagram of the VASO scan……..27

Figure 10. The middle slice of the VASO and CBV images of one subject……..28

Figure 11. Hand-drawn hippocampal subfiled ROIs……..30

Figure 12. VASO rCBV in combined hippocampal subfields in NC and SZ groups……31

Figure 13. rCBV in each hippocampal subfield in NC and SZ groups……31

Figure 14. The tagging scheme of balanced pCASL sequence……..33

Figure 15. PANSS positive score distribution (left) and PANSS total score distribution (right) in SZ-on and SZ-off groups in pCASL study……..35

Figure 16. Brain mask used for calibration in CBF calculation……36

Figure 17. FSL generated left and right hippocampal masks of one subject……..36

Figure 18. rCBF of left hippocampus in NC, SZ-on and SZ-off groups, and rCBF of right hippocampus in NC, SZ-on and SZ-off groups……37

Figure 19. Correlation between PANSS total score and hippocampal rCBF in SZ……..…37

Figure 20. Correlation between PANSS total score and hippocampal rCBF in SZ-off and SZ-on……..38

Figure 21. Demonstration of acquired Equivalence (AE) task with Training Phase (3 stages) and Transfer phase……..42

Figure 22. Stimulation AE tasks generated by E-Prime……..45

Figure 23. PANSS positive score distribution (left) and PANSS total score distribution (right) in SZ-on and SZ-off groups in AE study……46

Figure 24. Behavior results of Trained and Transfer tasks in NC and SZ groups……47

Figure 25. ROIs generated by WFU PickAtlas for AE ROI analysis……..48

Figure 26. Within group AE fMRI and ROI results……50

Figure 27. NC vs. SZ AE fMRI and ROI results……..51

Figure 28. NC vs. SZ good and poor AE fMRI and behavior results……..…52

Figure 29. Within group good and poor AE Transfer fMRI results……..…54

LIST OF TABLES

Table 1. Demographic characteristics of all the volunteers in ^{1}H-MRS study……..18

Table 2. Demographic characteristics of all the volunteers in VASO study……26

Table 3. Demographic characteristics of all the volunteers in pCASL study……34

Table 4. Demographic characteristics of all the volunteers in AE study……..47

LIST OF ABBREVIATIONS

aCBF	Absolute Cerebral Blood Flow
ACC	Accuracy of responses
AE	Acquired Equivalence
APD	Antipsychotic Drugs
ASL	Arterial Spin Labeling
AUC	Area Under the Curve
BOLD	Blood Oxygenation Level-dependent
CA	Cornu Ammonis
CBF	Cerebral Blood Flow
CBV	Cerebral Blood Volume
$CMRO_2$	Cerebral Metabolic Rate of Oxygen Consumption
Cr	Creatine
CRLBs	Cramer-Rao Lower Bounds
DA	Dopamine
DG	Dentate Gyrus
EPI	Echo-planar Imaging
ERc	Entorhinal Cortex

fMRI	Functional Magnetic Resonance Imaging
FDR	False Discovery Rate
FID	Free Induction Decay
FOV	Field of View
GABA	Gamma-Aminobutyric Acid
Gd-DTPA	Gadolinium Complex of Diethylenetriamine Pentaacetic Acid
Gln	Glutamine
Glu	Glutamate
Hippo	Hippocampus
^{1}H-MRS	Proton Magnetic Resonance Spectroscopy
iGluRs	Ionotropic Receptors
i.v.	Intravenous
LTD	Long-term Depression
LTP	Long-term Potentiation
mGluRs	Metabotropic Receptors
MPRAGE	Magnetization Prepared Rapid Gradient Echo
MTL	Medial Temporal Lobe
NAA	N-Acetyl-Aspartate

NC	Normal Control Volunteers
PANSS	The Positive and Negative Syndrome Scale
pCASL	Pseudo-Continuous Arterial Spin Labeling
ppm	Parts Per Million
PRESS	Point Resolved Spectroscopy Sequence
rCBF	Relative Cerebral Blood Flow
rCBV	Relative Cerebral Blood Volume
RF	Radio Frequency
ROI	Region of Interest
SCID	DSM-IV-TR Axis I Disorders
SNR	Signal To Noise Ratio
Sub	Subiculum
SZ	Schizophrenia
SZ-off	Off-Medication Schizophrenia Volunteers
SZ-on	On-Medication Schizophrenia Volunteers
T_1	Longitudinal Relaxation Time
T_2	Transverse Relaxation Time
TE	Echo Time

TR	Repetition Time
VASO	Vascular-Space Occupancy
VTA	Ventral Tegmental Area

CHAPTER ONE

Background

Schizophrenia

Schizophrenia is a chronic incapacitating syndrome that strikes about 1% of the population in the world. Another 2-3% of the general population has schizotypal personality disorder, which is often considered to be a milder form of the disease.[1] Schizophrenia symptoms characteristically begins during young-adult years, but cognitive disturbances are often evident earlier.[2,3] Profound psychosocial disability occurs, with only 15% of probands employed, 20% married and 5% recovered during their life time.[4] Schizophrenia is estimated to be the seventh most costly diseases because of the high frequency of hospitalization, need for psychosocial services and loss of productivity.[5,6] And there is no diagnostic test for schizophrenia; clinicians lack biological markers to define onset and follow illness progression; treatments are symptomatic and pathophysiology remains unknown.[7] The medical need for schizophrenia is high and increased understanding is imperative.

Schizophrenia is a diagnosis defined by behavioral presentation and illness course instead of a clear molecular pathophysiology as many other illness categories, and pharmacological treatments have been available only in the past half century.[8] It is characterized by three classes of signs and symptoms: psychosis (e.g., hallucinations, delusions, and thought disorder), cognitive dysfunction (e.g., reductions in attention, memory, and executive function), and negative symptoms (e.g., anhedonia, asociality and alogia). It has been postulated that different symptoms are associated with aberrant activity of distinct brain regions and/or neurotransmitters.

Psychosis defines schizophrenia and it has several distinct definitions in the Diagnostic and Statistical Manual of Mental Disorders, Fourth Edition Text Revision (DSM-IV-TR). The broader definition includes “other positive symptoms of schizophrenia (disorganized thought process, and grossly disorganized or catatonic behavior)” in addition to delusions and hallucinations,[9] and it is commonly used in making clinical diagnoses. After florid onset, psychotic symptoms often become milder with time, notably after the age of 50.[10] Psychosis is the target of current antipsychotic drugs (APDs), and APD pharmacology involves dopamine and other monoamine antagonism. Although APDs treat psychosis in schizophrenia well, considerable side effect and residual symptoms still remain. [11,12]

Cognitive dysfunction broadly impairs psychosocial recovery in schizophrenia, and it can exist in nearly psychosis-free schizophrenia patients. It mainly manifests impairment in attention, executive function, and working and declarative memory.[13] Cognitive dysfunction often begins before psychosis onset and persists evenly (without episodes) throughout the illness.[14] Cognitive disabilities are similar in acute and chronic schizophrenia, similar in adult- and adolescent-onset patients and similar in type (but not in degree) in family members and in high-risk, not-yet-ill persons.[15] Cognitive deficits only show small to moderate correlations with clinical state[16] and are not thought to change with APD treatment[17]. Since cognitive dysfunction is thought to be the most disabling and persistent feature of the illness, considerable research attention has been directed toward the correct articulation and effective treatment of it[18-20]. We mainly consider psychosis and cognitive symptoms (specifically memory), the two most common symptom complexes here.

Neuroanatomic basis of schizophrenia

Nissl stain, introduced by the German neurologist Franz Nissl, distinguishes neurons and glia from one another; it enables histologists to study the arrangement of neurons in different parts

of the brain. In 1873, Camillo Golgi discovered a potassium dichromate and silver nitrate stain that labeled individual neurons- soma, dendrites and axons- at random, supporting the idea that the brain was composed of individual cells.[21] Santiago Ramon y Cajal used Golgi's method to make exceptionally detailed drawings of brain anatomy which helped to establish that the brain consisted of individual cells termed "neurons".[22-24] Cajal proposed that information transferred between neurons using a directionally specific synaptic transmission. Both Golgi and Cajal were awarded the Nobel Prize in Physiology or Medicine in 1906.

Korbinian Brodmann was a German neurologist who analyzed the cortex of humans and other nonhuman primates. He divided the cerebral cortex into 43 distinct regions based on their cellular characteristics. Each region had its distinct cell types and cellular organization, and was called "Brodmann area" with a specific number.[25,26]

The neuronal synapse has two sides: presynaptic and postsynaptic. The usual direction of information flow is from presynaptic to postsynaptic. The presynaptic side generally consists of an axon terminal, while the postsynaptic side may be the dendrite or soma of another neuron. The information transfer at the synapse from one neuron to another is called synaptic transmission. Information in the form of electrical impulses traveling down the axon is converted into a chemical signal in the terminal that crosses the synaptic cleft. And then this chemical signal is converted into an electrical once again on the postsynaptic membrane, as well as into activity-dependent synaptic protein changes. The chemical signal is called a neurotransmitter which is stored in and released from the synaptic vesicles.

If we see the neurons under the microscope, about three-fourths of them are covered with little spiny bumps on their dendrites, while the rest are not. It turns out that these "spiny" neurons contain excitatory neurotransmitters such as glutamate (Glu), while the "non-spiny" ones contain inhibitory neurotransmitters such as gamma-aminobutyric acid (GABA)[27]. The neuron cells are also classified by their shapes, such as "pyramidal cells".

Biochemistry background of schizophrenia

Glutamate (Glu) is one of the 20 amino acids used to assemble proteins and the most abundant excitatory neurotransmitter in human brain. It accounts for neurotransmission in 100% of pyramidal neurons, virtually all cortico-cortical neurotransmission and approximately 60% of total brain neurons.[30] Glutamate mediates its neurophysiological effects through both ionotropic and metabotropic receptors and their activation gives rise to a postsynaptic current. Ionotropic receptors (iGluRs) which are linked to intrinsic ionic channels including the NMDA-, AMPA- and kainite-type. They form an ion channel that activates when glutamate binds to the receptor. Metabotropic receptors (mGluRs) are not directly associated with channels and are divided into groups in accordance with second messenger systems. They indirectly activate ion channels on the plasma membrane through a signaling cascade that involves G proteins. Both ionotropic and metabotropic glutamate receptors have been shown to have an effect on synaptic plasticity, a property of the brain thought to be vital for memory and learning.[31] An increase or decrease in the number of ionotropic glutamate receptors on a postsynaptic cell may lead to long-term potentiation (LTP) or long-term depression (LTD) of the cell respectively.[32,33] Metabotropic glutamate receptors may modulate synaptic plasticity by regulating postsynaptic protein synthesis through second messenger systems.[34]

Gamma-aminobutyric acid (GABA) is the most abundant inhibitory neurotransmitter in the brain. It plays a role in regulating neuronal excitability throughout the nervous system. It's synthesized from glutamate by the enzyme L-glutamic acid decarboxylase and pyridoxal phosphate as a cofactor via a metabolic pathway called the GABA shunt.[35.36] GABA acts at inhibitory synapses in the brain by binding to specific transmembrane receptors to cause the opening of ion channels. This action results in a negative change in the transmembrane potential, usually causing hyperpolarization. There are two classes of GABA receptors: $GABA_A$ and $GABA_B$.

$GABA_A$ ionotropic receptors are ligand-gated ion channels and $GABA_B$ metabotropic receptors are G protein-coupled receptors.

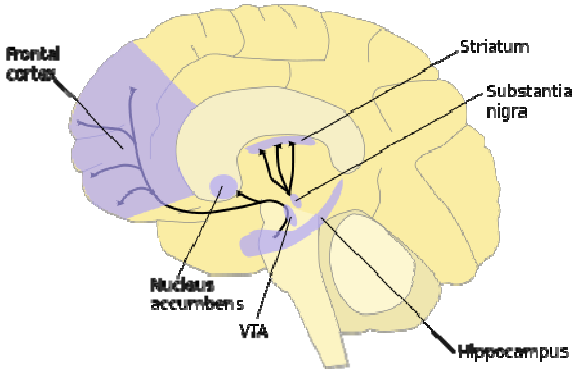

Fig 1. Dopamine Pathways. As part of the reward pathway, dopamine is manufactured in nerve cell bodies located within the ventral tegmental area (VTA) and is released in the nucleus accumbens and the prefrontal cortex. Its motor functions are linked to a separate pathway. Schizophrenia has been hypothesized to have elevated levels of dopamine activity in the mesolimbic pathway and decreased levels of dopamine in the prefrontal cortex.

Dopamine (DA) functions as a neurotransmitter in the human brain and plays important roles in behavior and cognition, voluntary movement, motivation, punishment and reward. It is synthesized within cells (mainly by neurons and cells in the medulla of the adrenal glands). Dopaminergic neurons are restricted to the midbrain, including the ventral tegmental area (VTA), the substantia nigra pars compacta and the arcuate nucleus of the hypothalamus. (Figure 1) The human brain has five known types of DA receptors. They are G protein-coupled receptors and labeled as D_1, D_2, D_3, D_4 and D_5. Upon synthesis, DA is transported from the cell cytosol into synaptic vesicles and stored there until an action potential occurs and forces them to merge with the cell membrane via exocytosis, thereby pumping DA into synapses. Once in the synapse, DA binds to and activates postsynaptic DA receptors, propagating the signal of the presynaptic neuron to the postsynaptic neuron. DA also binds to presynaptic DA receptors either exciting or inhibiting the presynaptic cell. After DA performs its synaptic duties, it is taken up back into the presynaptic cell.

The dopamine and glutamate hypotheses of schizophrenia

Because schizophrenia affects many of the characteristics that make us human: thought, perception, and self-awareness, understanding its neurobiological basis is one of the greatest challenges of neuroscience. There are two prevailing hypotheses of schizophrenia, both of which are related to our study: the dopamine hypothesis and the glutamate hypothesis.[37] Because the manifestations of schizophrenia are cognitively complicated, it may be that the illness includes brain systems that include both dopamine and glutamate.

According to the dopamine hypothesis of schizophrenia, psychotic episodes in schizophrenia are triggered specifically by the over-activation of dopamine receptors.[37] As one of the longest-standing hypotheses of schizophrenia, the dopamine hypothesis is based on multiple observations linking dopamine dysregulation to the pathophysiology of the disease. And substantial evidence suggests that psychosis in schizophrenia is related to dysregulation of subcortical dopamine system function. Study shows that this dysregulation is secondary to hyperactivity can occur within hippocampal subfields, and this hippocampal hyperactivity is associated with enhanced dopamine neuron activity and positive symptoms.[38]

Over the past 20 years, attention has turned increasingly to dysfunction of the brain glutamate system as a fundamental underlying pathophysiology in schizophrenia. Accumulating evidence supports a link between the NMDA system, disordered cognition and sensory processiong. According to the glutamate hypothesis, the schizophrenic disorder reflects diminished activation of glutamate signaling in the brain especially at NMDA receptors, an alteration that could be mediated through presynaptic, post-synaptic and/or related astrocytic proteins. Glutamate alterations within human brain are regional.

In our acquired equivalence (AE) study, we propose to test the effect of dopaminergic modulation on hippocampal activity. Meanwhile, we carried out a study trying to show that anti-dopamine medications (antipsychotics) also repair performance and function of the

hippocampus in schizophrenia. Our baseline CBV and CBF measurements in hippocampus using VASO and pCASL techniques will provide data on what are the basal levels of local activity in hippocampus and how this is related to clinical response to antipsychotic medication.

Hippocampus and schizophrenia

The hippocampus is one of the most extensively studied brain regions, and aspects of human memory mediated by hippocampus are well characterized. It is located in medial temporal lobe and is essential for the consolidation of long-term memories. The hippocampus consists of two thin sheets of neurons folded onto each other. One sheet is called the dentate gyrus, and the other sheet is called Ammon's horn. Of the four divisions of Ammon's horn, we will focus on two: CA3 and CA1 (CA stands for cornu Ammonis, Latin for "Ammon's horn"). Its component structures are arranged hierarchically and topographically.

The hippocampus receives convergent signals from neocortical regions, mediated through the parahippocampal and entorhinal cortex. The primary projection to the hippocampus comes from the entorhinal cortex then projects to hippocampus through the perforant pathway to the dentate gyrus. Dentate gyrus neurons give rise to axons (called mossy fibers) that synapse on pyramidal cells in CA3. The CA3 cells give rise to axons that branch. One branch forms the recurrent collaterals to other areas within CA3. The other branch called the Schaffer collateral forms synapses on the neurons of CA1.

Within the hippocampus, pyramidal layers are densely packed with glutamatergic excitatory neurons. Inhibitory interneurons containing GABA lie within the polymorphic layer and send their processes to modulate excitatory cell firing. The excitatory glutamate projections within the hippocampus have a low firing threshold, endowing the structure with a strong capacity for plasticity, advantaging learning and memory functions. The hippocampus is responsible for the

fast binding of inputs from multiple neocortical regions (conjunctive encoding), wherein the array of features that constitute an event are bound into an integrated, but flexibly addressable, memory trace,[40-42] and the subsequent retrieval of previously learned input patterns.[41, 43-45] At retrieval, conjunctive representations may permit associative recognition, inferential reasoning, and event recollection through pattern completion that results in retrieval of an extended representation from partial input. CA3 has extensive networks of recurrent collateral projections thought to be the anatomic substrate for the conjunctive encoding and pattern completion processes central to declarative memory. The dentate gyrus and, to a lesser extent, CA3 are thought to play a fundamental role in mediating pattern separation, wherein novel events that are similar to, but not exactly the same as, past events are established as unique hippocampal representations.[39]

A range of studies have established that the posterior extents of the hippocampal long axis are more likely to be involved in memory and cognitive processing, while the anterior extents of the hippocampal long axis are more involved in other complex behaviors such as stress, emotion, sensory-motor integration and goal-directed activity.[46-50] In schizophrenia patients, study has implicated that within the anterior aspects of the hippocampal long axis and, within the hippocampal circuit, changes were found in the anterior CA1 and subiculum. These studies also suggest that the left hippocampus is typically more affected than the right one in schizophrenia.[51,52]

Several lines of evidence show a decrease in hippocampal activation related to schizophrenia,[53,54,39] and further evidence for hippocampal dysfunction comes from structural imaging and post-mortem analyses demonstrating consistent anatomical differences (e.g. decrease in hippocampal volume) in schizophrenia patient brains.[55-57] However, a decrease in activation does not indicate a decrease in neuronal activity in hippocampal subregions. Actually, considerable literature demonstrates that activity at rest within distinct hippocampal subregions

is increased in brains of schizophrenia patients. High spatial resolution imaging techniques provide evidence for increased regional cerebral blood flow[58] and increased regional cerebral blood volume (dynamic susceptibility contrast MRI)[59] at rest in schizophrenia patients, and meaningfully, these increases have been directly correlated with clinical measures of schizophrenia psychosis[59,60].

Hippocampal metaplasticity model for schizophrenia

Metaplasticity is the plasticity of the synapse for LTP and LTD that adapts as a function of the average activity of the neuronal population; it is held to be a process which keeps the network of modifiable synapses within a set dynamic range.[61,62] The plasticity of a synapse (or of a population of synapses) can change, sometimes dramatically, in response to the history of prior synaptic activity. Speculatively, the proximal dentate gyrus molecular lesion in schizophrenia, with a reduction in mossy fiber excitatory activity, might create a leftward shift in metaplasticity within the CA3 subfield and an increase in LTP at CA3 synapses, an effect that would be magnified by the extensive excitatory recurrent collaterals within CA3.

The metaplasticity model around which we propose to examine the hippocampal changes in schizophrenia draws support from molecular findings in postmortem schizophrenia tissue as well as known medial temporal lobe (MTL) functional pathology. Evidence for reduction of glutamate transmission at the NMDA receptor has been found in schizophrenia previously,[63-66] but recent data predominately indicate reduced glutamate signaling in dentate gyrus. Postmortem molecular study in schizophrenia has found reduced transmission at the NMDA receptor specifically in dentate gyrus.[67-69] The effect that this proximal reduction in glutamate transmission has on downstream hippocampal projection fields (e.g., particularly on CA3) is precisely the mechanism we think might generate broader MTL pathology and psychosis. In animal models of LTP in MTL and visual cortex, if incoming sensory stimuli are reduced, the

threshold for induction of LTP falls, and lower amounts of sensory input generate more LTP.[70-74] We hypothesize that the pathological reduction in NMDA signaling in dentate gyrus in schizophrenia lowers the metaplasticity threshold onto its target, the CA3 neurons, generating heightened sensitivity to other incoming stimuli in CA3. This increased LTP would be expected to increase the associative function of CA3, under some circumstances (e.g., with increased afferent stimulation from modulating systems), thus the increased LTP would generate associative "mistakes", viz. psychotic productions and psychosis-induced interference with mnemonic function. (Figure 2) Moreover, the increase in LTP onto CA3 neurons and the consequent[75] increase in neuronal activity in CA3 could be propagated directly or negatively downstream to CA1.

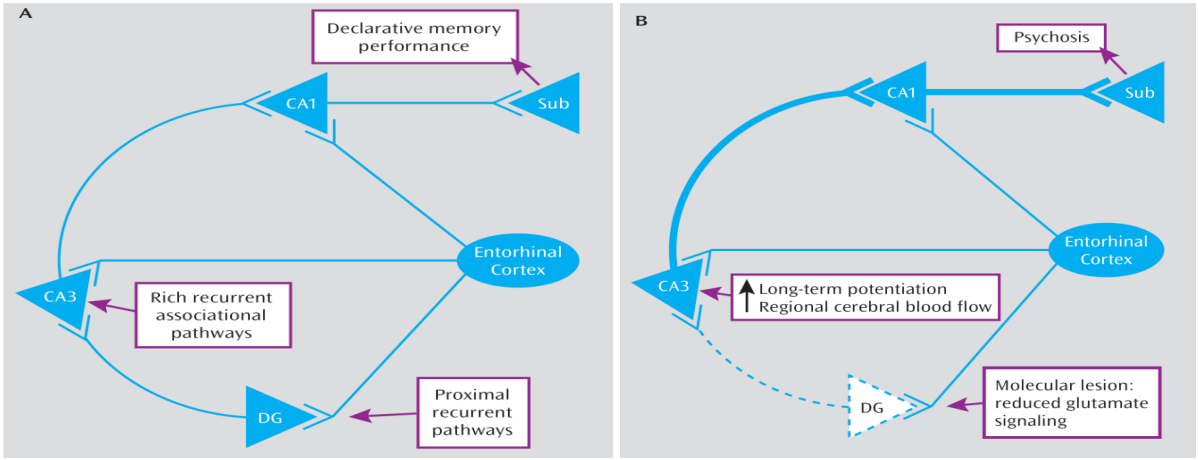

Fig 2. Hippocampal metaplasticity model for schizophrenia. A model of psychosis in schizophrenia which posits that neuronal activity is increased in CA3 due to reduced afferent innervation from DG and exaggerated plasticity responses within the CA3 recurrent collateral- and the direct perforant pathway-projections.[76]

Our testable model to describe the role of hippocampus in schizophrenia is based on two hypotheses. 1) A change in homeostatic plasticity processes in CA3 and CA1, accompanied by

increased activity due to reduced dentate gyrus glutamatergic output, could increase the pattern completion functions of CA3, resulting in memories with psychotic content. 2) The loss of mnemonic functions specific to the dentate gyrus, namely pattern separation, could increase the prevalence of illusory pattern completion and reduce discrimination between present and past experiences in memory.[39] Our Proton Magnetic Resonance Spectroscopy (^{1}H MRS), Vascular-Space-Occupancy (VASO), Pseudo-continuous Arterial Spin Labeling (pCASL) and functional Magnetic Resonance Imaging (fMRI) techniques, especially the high-resolution approaches, will help us to test this model.

CHAPTER TWO

Proton MRS measurement in hippocampus

Introduction

The dysfunctional brain circuits in schizophrenia involve multiple cerebral regions, including the hippocampus, the surrounding medial temporal lobe, anterior cingulate and prefrontal cortex .[39] Studies suggest that hippocampus engages early in the disease process that is persistent over the life course[77,78], with more alterations in the left hippocampus than in the right, and predominant changes were found in the hippocampal glutamatergic but not the GABA neurotransmitter systems[79-81].To investigate factors that contribute to the hypoglutamatergic state in schizophrenia, we used ^{1}H-MRS to measure the left hippocampal glutamate, GABA and other brain metabolite concentrations in normal and schizophrenia volunteers. We predicted a decrease in overall glutamate concentrations, particularly in the neurotransmitter pool. Since glutamate provides the major excitatory input in the hippocampus, we also predicted that the alterations in the excitatory afferents might be accompanied by changes in GABA concentration, the neurotransmitter in the inhibitory interneurons, which drives hippocampal inhibition. As an active control, we also measured the concentrations of N-acetyl-aspartate (NAA), an agonist of the mGluR3 receptor. NAA is reliably decreased in a large number of neuropathological brain conditions, including schizophrenia[34], stroke and Alzheimer's disease. A regional NAA decrease signals the presence of tissue pathology but lacks specificity in regards to the molecular or cellular alterations. As such, we predicted that hippocampal NAA concentration would be reduced in schizophrenia patients.

^{1}H-MRS method

MRS is an analytical method used to identify and quantify metabolites in samples. MR spectra can be obtained from different nuclei. Proton (^{1}H) is the most used nuclei for clinical applications in the human brain mainly because of its high sensitivity and abundance. ^{1}H-MRS is based on the chemical shift properties of the atom. When a tissue is exposed to an external magnetic field, its nuclei will resonate at Larmor frequency:

$$f = \gamma B_0 \qquad [1]$$

where B_0 is the actual strength of the magnet in units like tesla (T), and γ is the gyromagnetic ratio of the nucleus being tested which is calculated from its magnetic moment, spin number, nuclear magneton and the Plank constant. The chemical shift is the resonant frequency of a nucleus relative to a standard. Often the position and number of chemical shifts are diagnostic of the structure of a molecule. The chemical shift is usually expressed in parts per million and is calculated by the difference between a resonance frequency and that of a reference substance divided by the operating frequency of the MR scanner. The chemical shift position of a nucleus is therefore independent of the field strength. The MR spectrum is represented by the x axis that corresponds to the metabolite frequency in ppm according to the chemical shift and y axis that corresponds to the peak amplitude. Some metabolites have doublets, triplets or multiplets due to J coupling effects.

The ^{1}H-MRS acquisition usually starts with anatomical images, which are used to select a volume of interest, where the spectrum will be acquired. There are two basic types of in vivo spectroscopy: single-voxel and multi-voxel. In the single-voxel spectroscopy, the voxel is acquired from a combination of slice-selective excitations in three dimensions in space, achieved when a RF pulse is applied while a gradient field is switched on. The most popularly used single voxel spectroscopy technique is point-resolved spectroscopy (PRESS). In PRESS sequence, the spectrum is acquired using one 90^o pulse followed by two 180^o pulses. Each

pulse is applied with a different gradient field. The signal emitted from the voxel is a spin echo. To restrict the acquired signal to the voxel selected, spoiler gradients that dephase the nuclei outside the voxel are needed.

Research participants

Twenty-two volunteers with DSM-IV TR diagnosis of either schizophrenia or schizoaffective disorder and eighteen volunteers who neither had a history of psychiatric disease nor endorsed having first-degree relatives with a psychiatric history were recruited from the Dallas metropolitan area. Eight SZ volunteers were off medication (SZ-off) for at least 6 weeks prior to their MRS scan; these volunteers were not acutely psychotic and had elected not to take their medication. The fourteen on-medication SZ volunteers (SZ-on) were recruited from the same clinical care and referral sources and were not acutely or floridly psychotic too.

Informed consent was obtained for all participants in accordance with procedures approved by the UT Southwestern IRB. After that, the volunteers underwent a brief enrollment interview followed by a more thorough diagnostic workup that included a psychiatric history, the Structured Clinical Interview for DSM-IV-TR Axis I Disorders (SCID)[83], a urine toxicology screen, and the Structured Clinical Interview for the Positive and Negative Syndrome Scale (SCI-PANSS or PANSS).[84] Ratings for psychosis and other symptoms were obtained by two trained research coordinators.

MRI scans

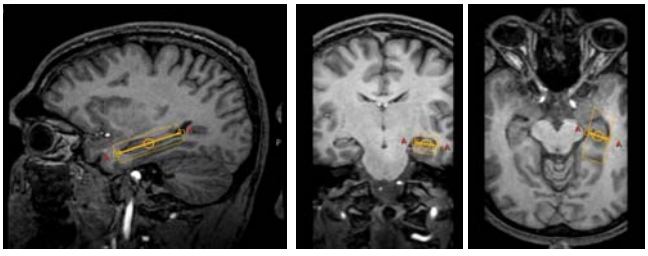

Fig 3. ^{1}H-MRS single voxel position. The 50×15×15 mm^3 voxel placed over the left hippocampus is shown in the sagittal plane (left image), coronal plane (middle image), and transversal plane (right image).

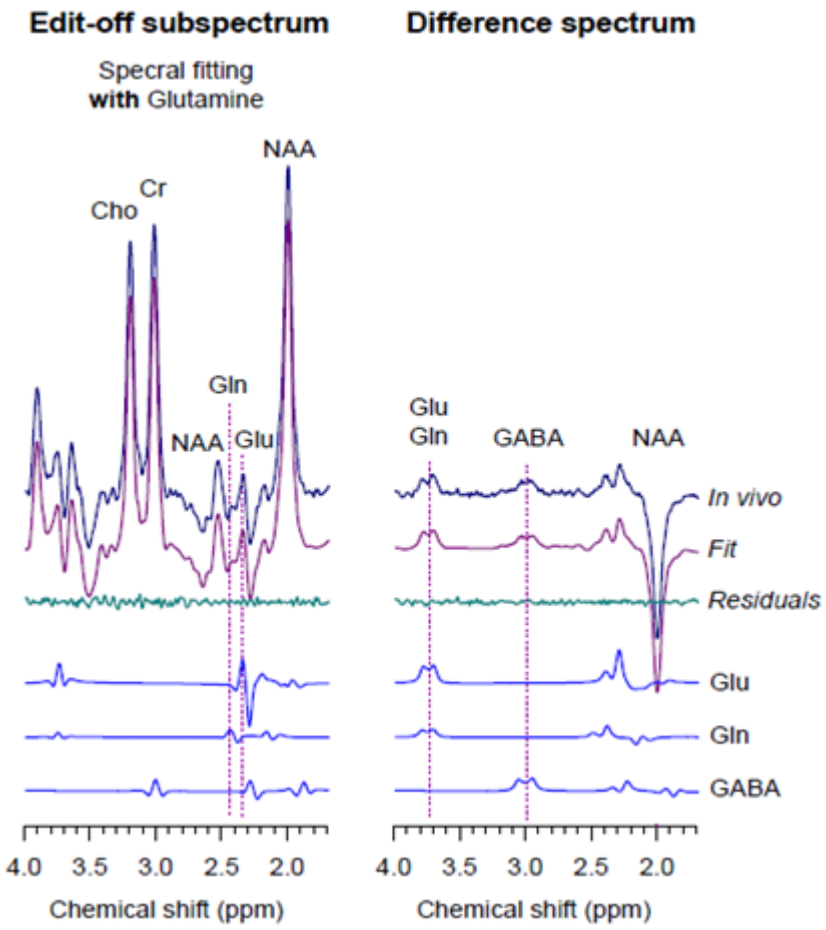

Fig 4. Typical spectrums acquired in this study. Left, edit-off subspectrum for glutamine assessment; right, difference spectrum for GABA assessment.

All the MRI experiments were carried out on a whole-body 3T Philips Achieva scanner. A standard birdcage head RF coil was used for signal transmission and reception. Magnetization prepared rapid gradient echo (MPRAGE) images were used for voxel positioning. (Figure 3) A single-voxel localized scalar (J) difference editing sequence was used for measuring GABA and glutamate.[85] A spectrally-selective 15-ms Gaussian editing 180° pulse (E180) (bandwidth = 76 Hz) was applied before and after the second 180° pulse of PRESS sequence. The E180 pulse was tuned to 1.9 ppm. Two spectra were obtained: one with E180 turned on (edit-on) and

another with E180 turned off (edit-off). A difference spectrum was obtained via subtraction of the edit-off spectrum from the edit-on spectrum. GABA was estimated from the difference spectrum and glutamine levels were assessed from the edit-off spectrum. (Figure 4) The total echo time of the MRS sequence was 70 ms, and the subecho times of the first and second slice-selective RF pulses were 25 ms and 45 ms respectively. Other MRS data acquisition parameters included TR = 2 s, number of averages = 512, sweep width = 2 kHz, and number of sampling points = 2048 (scan time ≈ 16 min). Edit-on and edit-off data were recorded alternatively in 128 blocks, each with 4 averages. The carrier frequency of the slice-selective RF pulses was set to 2.5 ppm. A variable-flip-angle four-pulse water-suppression scheme was applied prior to the editing sequence. Shimming of magnetic field was undertaken up to second order on the selected volume using FASTMAP method. An unsuppressed brain water signal was acquired from the same voxel under an identical gradient scheme for eddy current compensation. To avoid large head motions, each subject's head was immobilized with fitting foam padding and a head strap fastened across the forehead. To minimize frequency drifts during the data acquisition, a water signal following a low-flip angle (< 5°) excitation was acquired from the localized volume prior to each sequence run and the water resonance offset was determined and used for setting the synthesizer frequency (takes ~12 ms). With this method, the residual frequency drift during a 20-min scan was in most cases less than ±0.01 ppm.

MRS data analysis

The multi-block data were processed individually, corrected for eddy current artifacts and frequency drifts using an in-house Matlab program. Residual eddy current artifacts were removed using the unsuppressed brain water signal. Residual frequency drifts were corrected using the creatine 3.0 ppm singlet as reference. Following the summation of the spectra, LCModel software[86,87] was used to estimate the metabolite signals. The basis spectra for the

fitting were generated using density-matrix simulations, incorporating the spectrally-selective and spatially-selective RF and gradient pulses of the editing. The basis set included spectra of 17 metabolites: glutamate, glutamine, GABA, creatine, NAA, NAAG, glutathione, myo-inositol, scyllo-inositol, taurine, acetate, aspartate, ethanolamine, phosphoethanolamine, lactate, and glucose, and choline (glycerophosphocholine + phosphocholine). Published chemical shifts and J coupling constants[88] were used for calculating basis spectra. The spectral fitting was performed between 0.5 - 4.1 ppm. Cramer-Rao lower bounds (CRLBs), which indicate the goodness of the fit, were returned as a percentage standard deviation (%SD) with respect to the LCModel-estimated concentration. The metabolite concentrations reported here all have %SD less than 20%.

Primary analyses were conducted using two-sample Hotelling's t-square test to compare spectroscopic metabolic measurements in the two groups (normal controls – NC; schizophrenia volunteers - SZ). The threshold for significance set at $p \leq .05$ (uncorrected for multiple comparisons). Separate analyses were conducted for each metabolite: NAA, glutamate, and GABA. All values are reported as mean ± SEM (standard error of the mean).

Result

The demographic characteristics of the 18 NC and 22 SZ volunteers are presented in Table 1. Within the schizophrenia group, 14 subjects are SZ-on and 8 subjects are SZ-off. All the metabolite concentrations presented here were normalized by creatine concentration, so they are relative concentrations. To simplify the description, all the relative concentrations are referred to as concentrations here. Neither the glutamate nor the NAA concentration shows any difference between SZ-on group and SZ-off group, while GABA concentration shows a non-significant trend toward lower GABA levels in the SZ-on group. Furthermore, age did not

distinguish the SZ-on group from the SZ-off group. Therefore, we combined the SZ-on and SZ-off groups to compare with the NC group.

	Age	Sex	Medication
Normal Control (NC)	35±12	10 M, 8 F	18, off APD
Schizophrenia Volunteers (SZ)	42±11	18 M, 4 F	14, on APD 8, off APD

Table 1. Demographic characteristics of all the volunteers in ^{1}H-MRS study.

We assessed glutamate, NAA, and GABA concentrations in SZ (N = 22) in comparison to NC (N = 18). The glutamate concentration is significantly decreased in the SZ group. As predicted, there is also a significant decrease in NAA concentration between two groups. While GABA shows no significant difference between the two groups (Figure 5). Power calculation suggests that the NC and SZ groups are statistically sufficient for the two-sample Hotelling's t-square test used here. The lower Glu concentration in the SZ group comparing to the NC group can explain the decreased glutamatergic signaling in hippocampus in schizophrenia as hypothesized in our metaplasticity model. In schizophrenia, although we hypothesize a decrease in glutamate only in DG, we have tested our DG-selective NR1 KO mouse and show a decrease in glutamate, demonstrating that it is plausible to suggest that reduced MRS glutamate levels could derive from reduced DG glutamate.

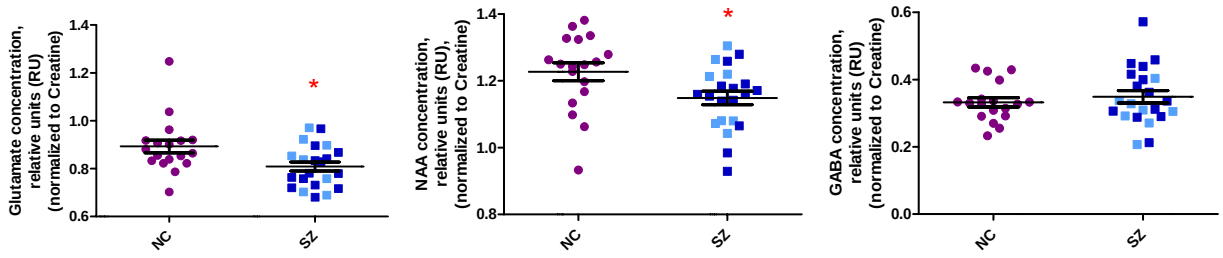

Fig 5. Glu (left), NAA (middle) and GABA (right) concentrations in the NC group (purple dots), and SZ group (blue squares). The SZ-off subjects are shown in light blue; the SZ-on subjects are shown in dark blue. The p values for two-sample Hotelling's t-square tests of Glu and NAA concentrations are 0.0133 and 0.0151 respectively.

Disscussion

The deep and lateral hippocampal location in human brain, as well as the field inhomogeneity surrounding the hippocampal tissue challenge probing the hippocampus for neurochemical data. The voxel boundaries extending beyond the hippocampus into parahippocampal tissue also vary from subject to subject. Consequently, only a few studies have examined hippocampus in schizophrenia using MRS, and the results are divergent.[89-92] To further assess Glu concentration within grey matter only in hippocampus, we used grey matter fraction in the voxel as a covariate in the t-test for NC and SZ group comparison. Significant decrease of Glu/Cr concentration was found in SZ group ($p = 0.0106$). Our findings of ^{1}H-MRS indicate that

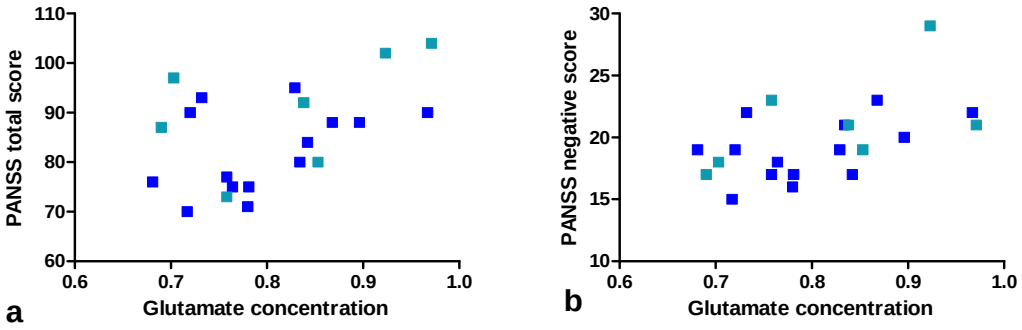

Fig 6. Glutamate correlations with the PANSS total score (a) and PANSS negative score (b) within the SZ group. The SZ-off subjects are shown in light blue; the SZ-on subjects are shown in dark blue.

schizophrenia is associated with reduced hippocampal glutamate concentrations. Moreover, glutamate concentrations correlate with the PANSS total and negative scores (figure 6), suggesting their relevance to disease manifestations. This effect is significant across all SZ volunteers, with no differences between the SZ-ON and SZ-OFF groups. We do not know what would be the contribution of hippocampal glutamate to negative symptoms nor are negative symptoms included in our model, but it seems the magnitude of glutamate reduction is related to

the negative symptoms. However, this is an outcome that we did not predict, it is merely an observation. Glutamate concentration measured by MRS is a combination of both the neurotransmitter and the metabolic pool which are known to be in a linear relationship with a slope of approximately 1[93,94], indicating that alterations in the total glutamate are likely to reflect equal changes in both the metabolic and the neurotransmitter pool. Under this assumption, the decreased hippocampal glutamate concentration in schizophrenia suggests that lower concentrations of glutamate are available for neurotransmission. The hippocampus is a multilayered complex structure whose anatomical details are not captured by these spectroscopic measures. An overall decrease of glutamate concentration in hippocampus cannot represent the decrease of glutamate concentration in all the hippocampal subfields.

A reduction in NAA is found in the schizophrenia patients as compared to the normal subjects. As one of the most abundant cerebral metabolites that can be the reliably detected in brain[97], NAA has long been hypothesized to be a marker of neuronal health and viability. Most published NAA studies in schizophrenia by MRS have reported a regional decrease of approximately 5 - 10% in several brain regions, including the hippocampus, prefrontal lobe, basal ganglia, thalamus, and the anterior cingulated, with most reliable findings of NAA reduction in hippocampus and prefrontal cortex[98].

We found no difference of GABA concentrations between the two studied groups, which may suggest no regulation of inhibitory transmission in schizophrenia. An alternative explanation is the lack of sensitivity of current available spectroscopic methods for GABA measurement, especially given the volume averaging of parahippocampal tissue in the relatively large voxel used here. Given the low GABA concentration, the metabolite needs to be measured at a relatively short TE, where macromolecule contamination is still significant.

No other study examined the effect of antipsychotic drugs (APDs) on the hippocampus, therefore ours is the first to demonstrate that chronic antipsychotic drug treatment has no overall

effect on hippocampal glutamate, NAA or GABA. Most likely, the medication effect is a function of time as well, since the long period required to achieve a visible clinical benefit is a well-known property of antipsychotics.

We have demonstrated ourselves that the metabolites we measured did not correlate with age in the hippocampus. Furthermore, no variation correlated with age has been demonstrated in the literature in the hippocampal glutamate concentration as measured by MRS. We now know that there are several subtypes of schizophrenia, that schizophrenia progresses with age, and that medications affect the course of the illness. Future studies should take these factors into account. And in ^{1}H MRS, the Cr peak represents Cr and phosphocreatine (PCr). PCr is a reservoir of energy for brain cells. It has been shown in several psychiatric illnesses that Cr levels may be pathologically altered. Thus, using Cr as a reference should be careful. In patients with schizophrenia, Cr may be reduced in anterior cingulate cortex. [99,100]

Future 7T experiment

We have started an ^{1}H-MRS study on 7T Philips scanner. A voxel placed in the anterior cingulate cortex and a voxel placed in the dorsal lateral prefrontal cortex will be used to measure Glu, Gln, NAA and GABA in NC and SZ subjects. The analysis of DLPFC and ACC, which are projection sites of hippocampus, will help us understand the alterations in these regions which are generated by fundamental dysfunction in hippocampus. Since the chemical shift (ppm) is independent of B_0, ^{1}H peak separation is also independent of B_0. The apparent decrease in singlet linewidths in ppm at high B_0 is direct and unequivocal evidence for increased spectral resolution in vivo at high field.[101] High field MRS will provide improved spectral resolution for J-coupled metabolites, because the coupling strength (Hz), which governs the overall linewidth of multiplets, is independent of the field strength. As the spectral pattern of coupled resonances changes with TE as a result of scalar evolution effects, the multiplets may

be narrowed with TE optimization, enhancing the specificity of the signals, with an additional advantage that the MM signals are suppressed to noise levels at long TE. Although the SNR is reduced as a result of T_2 relaxation, improved intermetabolite discrimination on a clean background can be achieved at an optimized long TE. With the benefits of increased chemical shift dispersion (Hz) and signal gain at high field, a TE-optimized acquisition may provide an efficient tool for the measurement of the low abundance coupled-spin metabolites with improved precision. A prior study has demonstrated that the PRESS TE, (TE_1, TE_2) = (37, 63) ms, enables reliable measurements of Glu and Gln at 7T. The numerically calculated PRESS spectra incorporating T_2 = 130ms at 7T indicates that the selectivity of the small GABA signal at 2.28 ppm, which is close to the abundant Glu multiplet, is also increased at this TE. The GABA multiplet amplitude of PRESS is 73% relative to 90º acquisition, ignoring T_2 effects. The linewidth of this GABA multiplet is approximately twofold smaller than that of a 90º acquisition.[102] The metabolite concentrations measured in ACC and DLPFC at 7T are more reliable compared to 3T. A test-retest study will also be conducted to verify the stability of the 7T ^{1}H-MRS method for our future drug study. It is hard to measure hippocampus at 7T because of its deep location in the human brain. The RF field inhomogeneity provided by our 16 channel coil limits the MRS measurement at hippocampus at 7T. However, this problem may be resolved through RF power calibration using RF coils with fewer channels. A uniform and ideal RF field can be achieved in the voxel covering the hippocampus this way.

Acknowledgment: The 3T MRS work was done by Ana D. Stan, Yan Fang, Perry Mihalakos, John J. Bartko, Stephanie U. Morris, Changho Choi, Carol A. Tamminga. I'm responsible for the preparation of the statistical analysis of the final ^{1}H MRS results. We acknowledge the following

grant support: R21 MH093959 (PI: Changho Choi, PhD), RO1 MH 83957 (PI: Carol Tamminga, MD), NARSAD distinguished investigator grant (PI: Carol Tamminga, MD).

CHAPTER THREE

CBV and CBF measurements in Hippocampus

A. VASO study

Introduction

Using our hippocampal metaplasticity model, we examine the prediction of the model that hippocampal subfield activations and perfusion will differ in NC, SZ-on and SZ-off groups, especially in dentate gyrus and CA3. Because the model of pathophysiology we have proposed in hippocampus invokes distinct activations in hippocampal subfields and distinct correlates between hippocampal subfields and schizophrenia symptoms, we carry out high resolution imaging for perfusion with Vascular Space Occupancy (VASO) measuring CBV in schizophrenia with (SZ-on) and without (SZ-off) treatment, contrasting both groups with NCs. VASO is used to assess high-res CBV focused on hippocampal subfields during rest. We predict a reduction in DG CBV, and increase in CA3 CBV and increase in CA1 CBV, albeit less so than CA3. The prediction indicates decreased basal neuronal activity in DG and increased basal neuronal activity in CA3 and CA1. We further hypothesize that this increased CBV will be reduced with APD treatment (but not entirely normalized). In the SZ-off, we predict a direct correlation between psychosis and CA3 perfusion and a loss of that correlation (due to a medication confound) in the SZ-on.

High-resolution VASO method

Quantitative determination of CBV is important for understanding brain physiology and pathophysiology. The dynamic susceptibility contrast MRI approach for measuring CBV employs a paramagnetic contrast agent (Gd-DTPA, gadolinium complex of diethylenetriamine pentaacetic acid) administered i.v. and uses a rapid image acquisition sequence to monitor the MR signal intensity during the first pass of the agent through the microvasculature[103]. This approach has the advantage of relatively high spatial resolution and low invasiveness. In our study, VASO MRI, a blood-nulling pulse sequence, in combination with the T_1 shortening

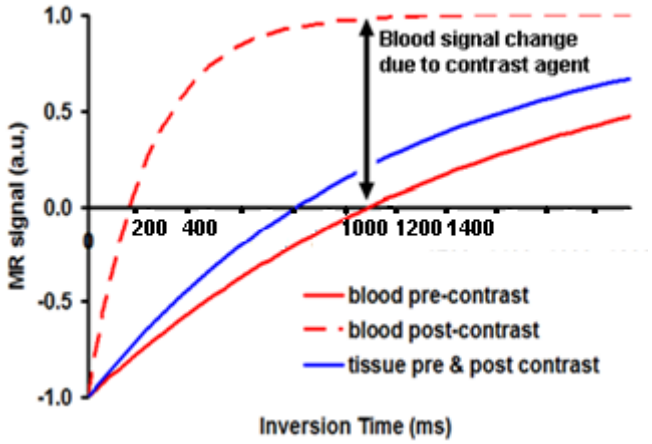

Fig 7. Inversion recovery curves for three proton species with different T_1 values at 3 T. Blood pre-contrast $T_{1,b}$ = 1624 ms. The blood magnetization is nulled without contrast agent and is fully recovered with contrast agent at TI = 1088 ms. Therefore, the signal difference between post- and pre- contrast images is proportional to the amount of blood present in the voxel.

property of Gd-DTPA, is used to accurately measure CBV. Two VASO experiments with identical imaging parameters are performed before and after contrast agent administration. Since the T_1 shortening effect of the contrast agent is confined to the blood compartment, the T_1 weighting of the tissue MR signal does not change between the two VASO experiments, whereas that of the blood changes from null to almost maximal signal. (Figure 7) The CBV map can be calculated directly from the signal difference between post- and pre-contrast VASO images with a correction factor.

MRI scans

A group of normal (NC; n=24) and patient volunteers, both medicated (SZ-on; n=22) and unmedicated (SZ-off; n=15), were studied. The demographics of this study are shown in Table 2. Significant difference between SZ-on and SZ-off groups in PANSS positive scores and PANSS total scores has been found. (Figure 8)

	age	education	gender	PANSS pos	PANSS total
NC	39±11	14±2	16M/8F		
SZ-on	39±10	13±2	16M/6F	18±4	69±11
SZ-off	37±10	13±3	11M/4F	22±5	80±19

Table 2. Demographic characteristics of all the volunteers in VASO study.

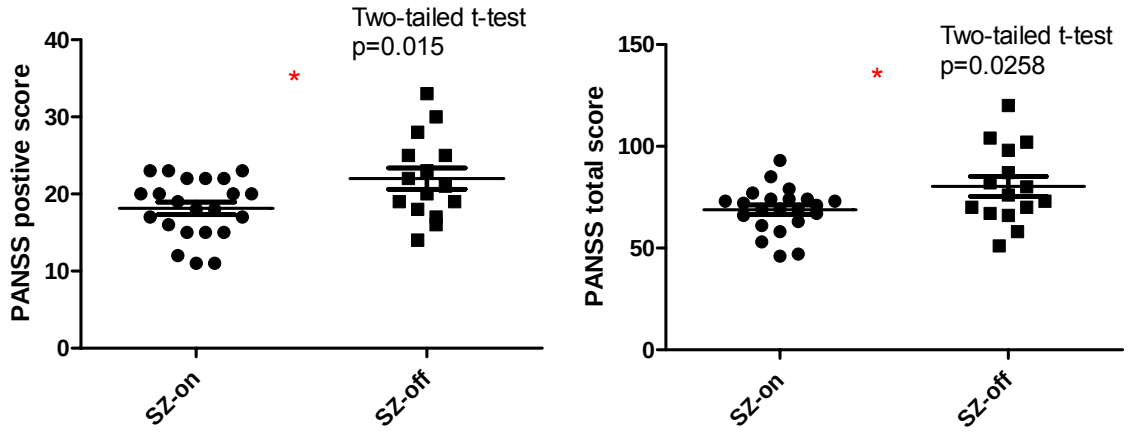

Fig 8. PANSS positive score distribution (left) and PANSS total score distribution (right) in SZ-on and SZ-off groups in VASO study. PANSS pos and PANSS total are both significantly higher in SZ-off comparing to SZ-on.

All the scans were done in a 3T whole-body Phillips scanner. For signal reception, an 8-channel SENSE head coil with parallel imaging capability was used. To assess perfusion, we used the VASO technique[104] to measure CBV. The VASO scan consisted five 2'30" dynamics (pre1, pre2, pos0, pos1, pos2), and Gd-DTPA (0.1mmol/kg, Magnevist ®) was injected at the beginning of pos2. (Figure 9) Coronal VASO images were acquired perpendicular to the hippocampus with an in-plane resolution of 0.78 mm x 0.78 mm and 9 4mm slices. (Figure 10) The TR and TI of the VASO scan are 6000 ms and 1088 ms respectively. The CBV map was calculated from the difference between post- and pre-contrast VASO images. A T2-weighted anatomical image with a high resolution (0.47 x 0.47 x 2 mm^3) was also acquired.

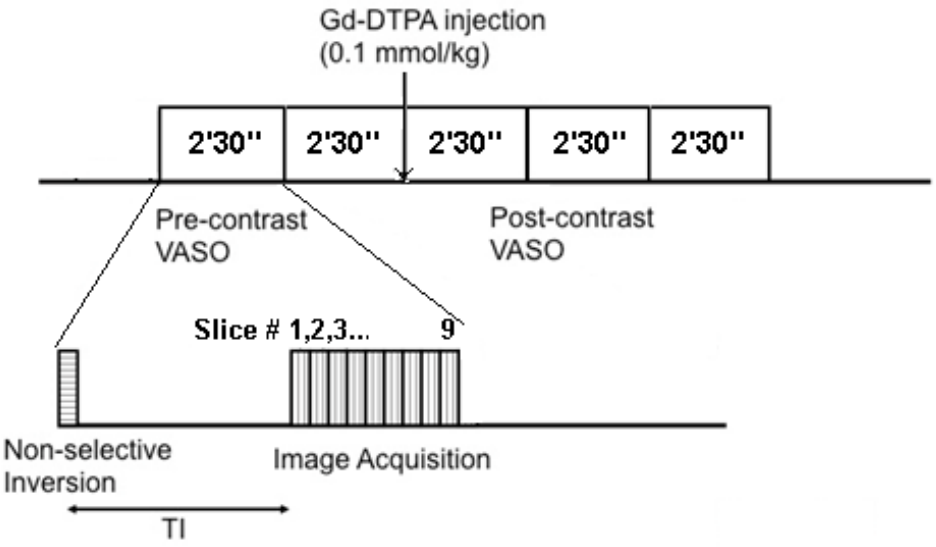

Fig 9. Timing diagram of the VASO scan. Five 2'30" dynamic scans (pre1, pre2, pos0, pos1, pos2) are acquired with the contrast agent injected at the beginning of the first post-contrast scan. A global inversion is followed by an optimal TI to null the pre-contrast blood signal.

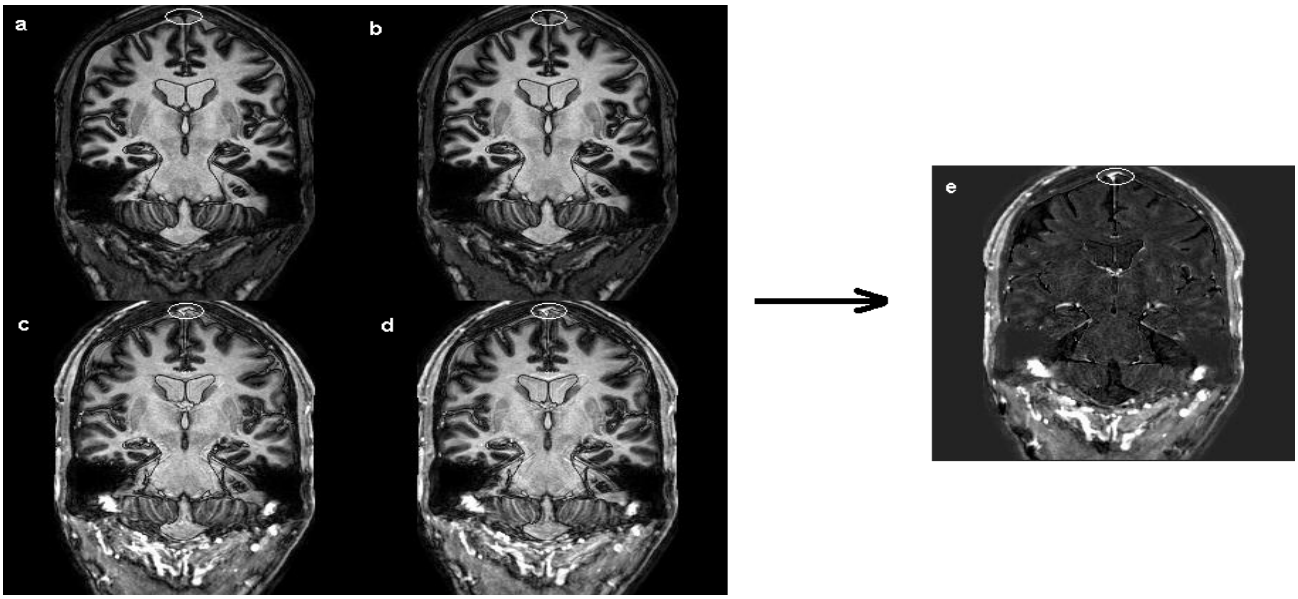

Fig 10. The middle slice of the VASO and CBV images of one subject. Sagittal Sinus area is circled on each image. (a) First pre-contrast VASO image (pre1). (b) Second pre-contrast VASO image (pre2). (c) First post-contrast VASO image (pos1). (d) Second post-contrast VASO image (pos2). (e) CBV map calculated from (pos1+pos2)/2-(pre1+pre2)/2 multiplied by a correction factor. The difference of sagittal sinus signal between post- and pre-contrast VASO images can be seen clearly in the circled area.

VASO data analysis

The CBV weighted (CBVw) map was calculated from the difference between the post- and pre-contrast images multiplied by a correction factor as the following equation.

$$CBVw = \left(\frac{pos1+pos2}{2} - \frac{pre1+pre2}{2}\right) \times \left(2e^{\left(-\frac{T_{acq}}{T_{1,b}}\right)} - e^{\left(-\frac{TR}{T_{1,b}}\right)}\right) \times (-1) \qquad [2]$$

Here $T_{acq} = TI + n_{slice} \times T_{gap}$, T_{gap} is the time between two adjacent slice acquisitions, TI is inversion time and it is 1088 ms at 3T, n_{slice} is the slice number. TR is 6000 ms and $T_{1,b}$ is whole blood T_1 at 3T and it is 1624 ms.

Hippocampal subfields including dentate gyrus (DG), subiculum (Sub), CA1, and CA3, were identified on the T2-weighted image using 3DSlicer 3.6 (http://www.slicer.org/). (Figure 11a)

ROIs of the hippocampal subfields were drawn by hand onto each slice of hippocampus on the T2 image between the head and tail of the hippocampus for both hemispheres. The registered CBV map was generated through spatial registration between the pre2 VASO image and the T2-weighted anatomical image performed by Statistical Parameter Mapping (SPM2) software (http://www.fil.ion.ucl.ac.uk/spm/software/spm2/) and in-house Matlab programs. Due to the remaining mismatch between registered CBV map and T2-weighted anatomical image, both images were segmented into small boxes covering all the hippocampal subfields, together with the ROI mask overlaid on each image (using the same coordinates). (Figure 11b) Then the reduced rCBV map was registered to the reduced T2-weighted anatomical image again. However there might still be some minor mismatch between the segmented ROI masks and the registered segmented rCBV maps. So we shifted the segmented ROI masks manually with a MATLAB program to best match the registered reduced CBV maps with the ROI masks. The mean VASO value of each ROI was calculated with a MATLAB program. The image fitting and analysis was done blind to subject group. We also excluded the voxels with negative values which might be caused by the CSF phase effect. To make the VASO CBV value more comparable between different subjects, a thalamus ROI mask drawn on the registered CBV map was used to get a mean thalamic CBV value for each individual. The medial regions of thalamus on the most posterior three slices available were chosen for ROI drawing. Then the mean thalamus CBV value was used to scale each hippocampal subfield CBV value. We originally used sagittal sinus CBV value as the scaling factor, but due to the large variation of the pure blood signal in sagittal sinus among subjects, we decided to choose thalamus (most grey matter) CBV value as the scaling factor. The Matlab programs used to calculate rCBF values can be found in Appendix A.

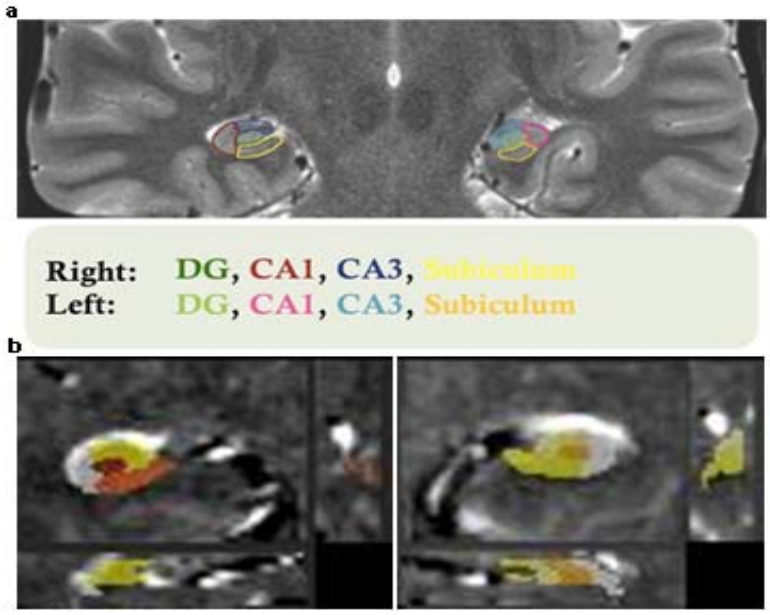

Fig 11. Hand-drawn hippocampal subfiled ROIs. (a) Hippocampal subfield ROIs on high resolution T2 image, labeled with different colors. (b) Segmented CBV maps overlaid with hippocampal subfield ROI masks for analysis.

Result

The hippocampal subfield CBV value is scaled by the thalamus CBV value and then multiplied by 100. The two group relative CBV (rCBV) values for left CA3+CA1+sub are shown in Figure 12. We have found no significant difference between SZ-on and SZ-off rCBV values, so we combine these two groups to compare with NC group. The mean rCBV value of SZ groups is significantly higher than NC group in left CA3+CA1+Sub. However, if we combine left DG with left CA3, CA1 and Sub, the significance is lost. (Figure 12) This can be explained by the large variance in DG rCBV. It may also suggest that the increase of rCBV in hippocampus is a subregional effect.

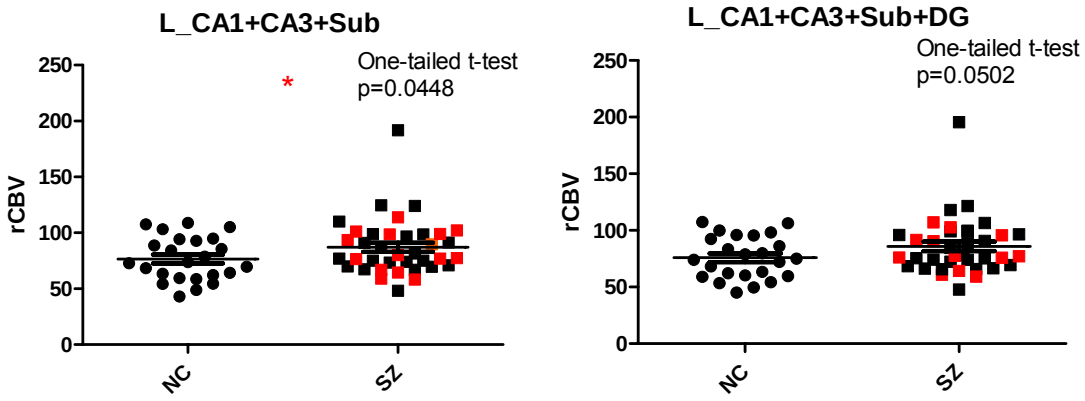

Fig 12. VASO rCBV in combined hippocampal subfields in NC and SZ groups. Left, Elevated rCBV in left CA3, CA1 and Sub by one-tailed, unpaired t-test (p = 0.0448). Right, No significant difference between NC and SZ in left CA1, CA3, Sub and DG. In SZ group on both graphs, black is SZ-on and red is SZ-off.

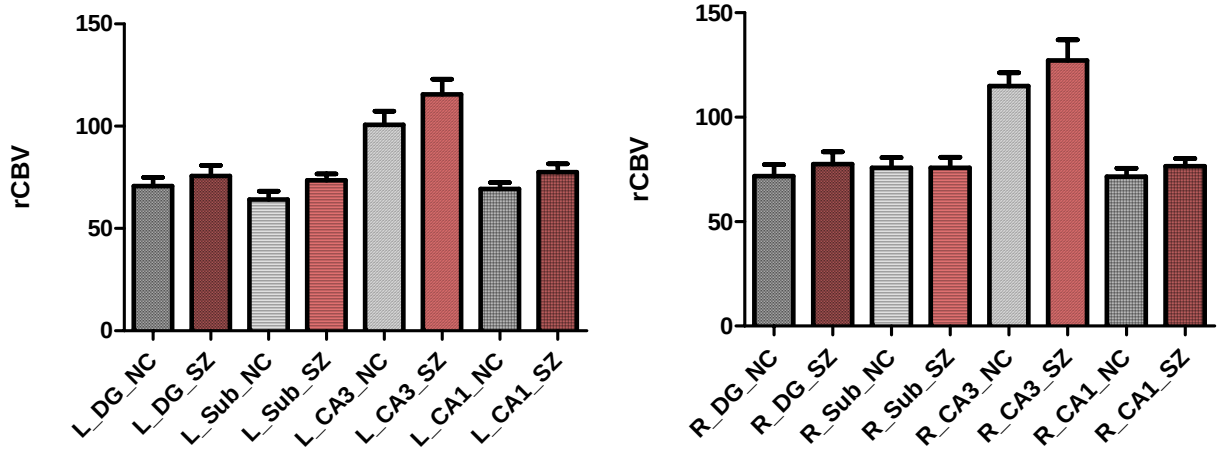

Fig 13. rCBV in each hippocampal subfield in NC and SZ groups. Left graph, rCBV of all the four left ROIs (DG, Sub, CA3, CA1) in NC and SZ groups. Right graph, rCBV of all the four right ROIs (DG, Sub, CA3, CA1) in NC and SZ groups.

Discussion

The majority of our VASO results affirms our predictions from the hippocampal metaplasticity model that perfusion is increased in CA3 and CA1 in SZ group comparing to NC group. Baseline CBV levels in hippocampus vary by subfields, with the highest CBV levels in CA3, which is an intriguing observation. (Figure 13) The elevation of basal CBV levels in CA3 in SZ group comparing to NC group suggests that a basal hypermetabolic state exists in hippocampus in schizophrenia. Basal metabolic increases in the medial temporal lobe or hippocampal formation that are associated with symptoms of psychosis have been shown in most published single-proton emission computed tomography.[105,106] Only a few studies have measured perfusion in hippocampal subfields in NC and SZ subjects, and our result is consistent with the only published study, which was not in high resolution format[59]. Due to the small hippocampal subfield ROIs and low SNR of the high resolution CBV maps, the user-guided ROI drawing on the high resolution T2-weighted images, and CBV maps coregistration with the T2-weighted image can result in some mismatching mistakes, although we try to avoid them through segmented image coregistration and manually shifting masks.

We have extended our hippocampal tissure analysis in postmortem SZ vs NC Hipp subfield tissue and find outcomes that have supported and expanded the metaplasticity model: (1) reduced GluN1 in DG are consistent with reduced excitatory transmission in the Mossy Fiber pathway (SB); (2) The elevation of GluN2B-containing NMDA receptors in CA3/CA1 suggest a homeostatic increase in tissue excitability (available upon request); (3) no change in AMPAR subunits or presynaptic trafficking proteins localizes the molecular target to the NMDAR; (4) elevated BDNP mRNA in st. oriens (ie, in the recurrent collateral insertion), suggests that autoassociation generally ascribed to this system could be dysfunctional in psychosis (SB); (5) The Golgi staining of human CA3 neurons shows evidence of increased synaptic strengthen (increased spines and dendritic complexity), directly supportive of the Model. We interpret these findings to suggest increased glutamatergic firing and firing instability within CA3 and increased

signaling within and downstream from pyramidal neurons in CA3. Certainly, an increase in firing within CA3, impinging on neurons within CA1 would generated overall circuit alterations and have profound functional implications for memory functions, those performance dysfunctions that we report in our AE study.

B. pCASL study

Introduction

Arterial spin labeling (ASL) is a noninvasive MRI tool and can be used for baseline neural activity measurement. Without exogenous agent injection, ASL has the potential to provide a quantitative assessment of CBF within 5 to 10 minutes. It magnetically tagging the protons in arterial blood, and then images mapping the vascular distribution of those feeding arteries are acquired. We used Pseudo-Continuous Arterial Spin Labeling (pCASL) technique to get the whole brain CBF map.[148] pCASL is a relatively new ASL technique which takes advantage of the superior SNR of continuous ASL and the high tagging efficiency of pulsed ASL. It employs a train of discrete RF pulses to mimic flow-driven adiabatic inversion during labeling session. There are two methods about pCASL, “unbalanced” pCASL and “balanced” pCASL. Here we used “balanced” pCASL for our study, which has identical tag and control gradient waveform with a residual net moment per cycle.[149]

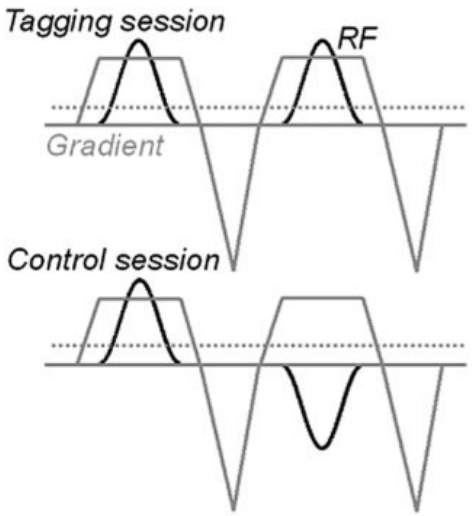

Fig 14. The tagging scheme of balanced pCASL sequence. RF polarity is constant during tagging session and alternated in control session. The zeroth gradient moment between two consecutive RF pulses is identical in tagging and control sessions.

MRI scans

pCASL scans were conducted on 3T Philips MR system. A group of 18 NC, 28 SZ-on and 18 SZ-off volunteers were studied. The demographics of this study are shown in Table 3. Significant difference between SZ-on and SZ-off groups in PANSS positive scores and PANSS total scores has been found. (Figure 15)

	age	education	gender	PANSS pos	PANSS total
NC	41±10	14±2	13M/5F		
SZ-on	39±11	12±3	21M/7F	19±5	71±15
SZ-off	38±10	14±3	13M/5F	23±6	82±18

Table 3. Demographic characteristics of all the volunteers in pCASL study.

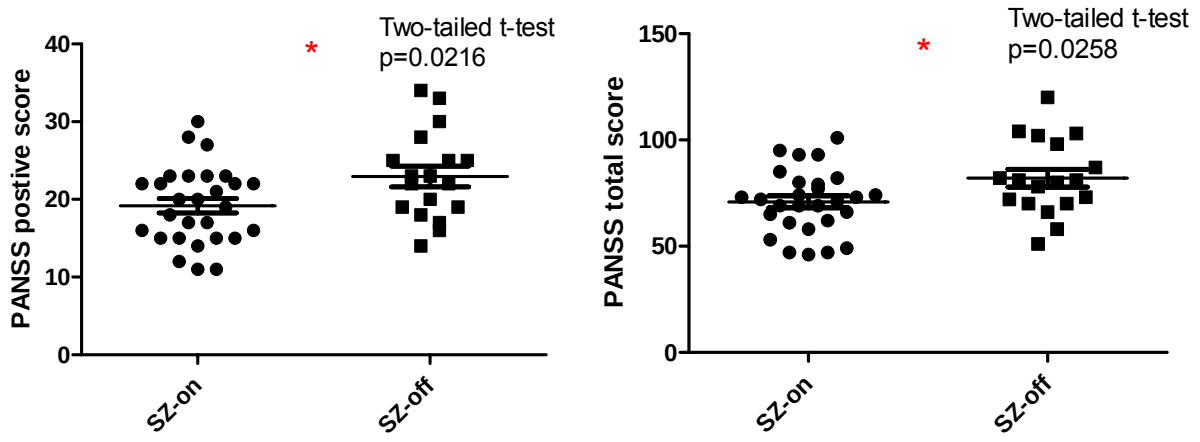

Fig 15. PANSS positive score distribution (left) and PANSS total score distribution (right) in SZ-on and SZ-off groups in pCASL study. PANSS pos and PANSS total are both significantly higher in SZ-off comparing to SZ-on.

Imaging parameters for pCASL sequence were: single-shot gradient-echo EPI, matrix = 80×80, voxel size = 3×3 mm^3, 27 slices, 5 mm slice thickness. Labeling duration = 1650 ms, post labeling delay = 1525 ms, TR = 4020 ms, TE = 13.79 ms. Acquisition delay between adjacent slices is 35 ms, number of controls/labels = 30 pairs. In addition, a time-of-flight (TOF) angiogram and a phase-contrast (PC) velocity MRI were performed to visualize the internal carotid arteries and vertebral arteries and correctly position the PC velocity MRI slice, and obtain absolute CBF values following previous procedures.[150] MPRAGE image with 1×1×1 mm^3 voxel size and 256×256×160 matrix was also acquired.

pCASL data analysis

The Pcasl control and label images were realigned first using SPM2 and Matlab. Then 30 difference images were calculated for each control and label pair and averaged. Slice timing correction was applied for different post-labeling delay times for different brain slices. In the

mean difference image, an axial brain slice across the thalamus was used to draw the brain mask covering the brain tissues (Figure 16), and the averaged voxel pCASL value was calculated. The pCASL signal for each voxel was calibrated using conversion constant between pCASL MRI signal and the physiologic unit to yield absolute CBF (aCBF) maps. The aCBF maps were then calibrated to generate the relative CBF (rCBF) maps. For details of aCBF and rCBF map calculation, please check Appendix B.

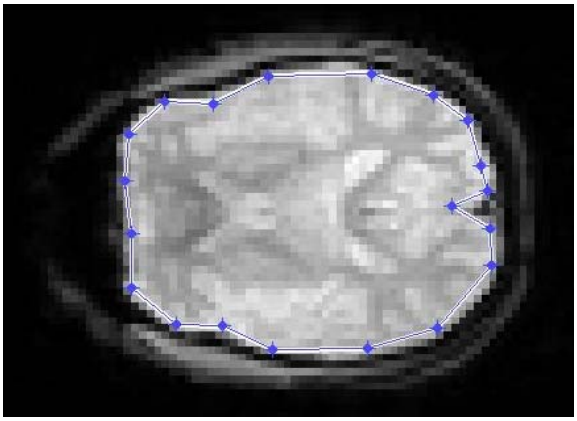

Fig 16. Brain mask used for calibration in CBF calculation. It is manually drawn on the axial slice across thalamus.

Afterward, the MPRAGE and the aCBF and rCBF maps of each subject were normalized to MNI space in SPM5 (http://www.fil.ion.ucl.ac.uk/spm/). Whole hippocampus mask of each individual subject was drawn using FSL 4.1.7 (http://www.fmrib.ox.ac.uk/fsl/) (Figure 17). Finally, the mean rCBF values within each hippocampal mask was calculated using 3DSlicer3.6.

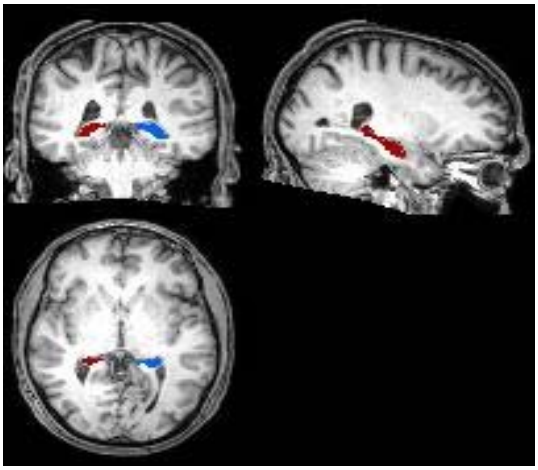

Fig 17. FSL generated left and right hippocampal masks of one subject. The background brain has been normalized to MNI space and is used to generate the hippocampal mask.

Result

With large variance and close means of rCBF values in NC, SZ-on and SZ-off groups, no significant difference was found between the three groups with one-way ANOVA or between NC and SZ groups with unpaired ttest. (Figure 18) However, when we check the correlation between left and right hippocampal rCBF and PANSS scores, it is significant for PANSS total scores. (Figure 19)

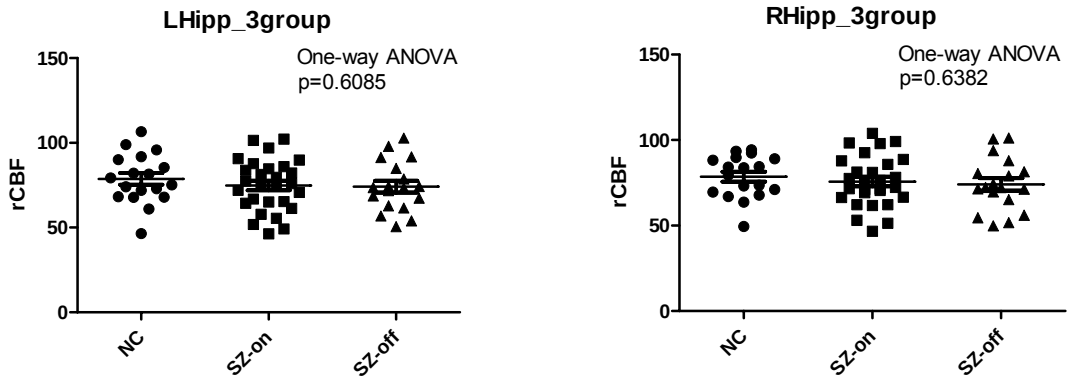

Fig 18. rCBF of left hippocampus in NC, SZ-on and SZ-off groups (left), and rCBF of right hippocampus in NC, SZ-on and SZ-off groups (right). No significant difference was found between NC, SZ-on and SZ-off groups in either left hippocampus or right hippocampus.

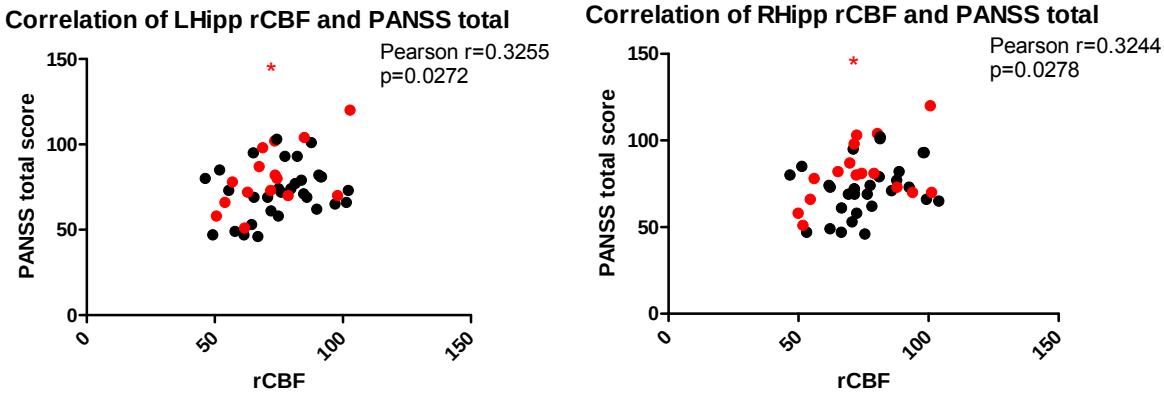

Fig 19. Correlation between PANSS total score and hippocampal rCBF in SZ. Pearson correlation between left hippocampal Rcbf of SZ group and PANSS total scores (left) and between right hippocampal Rcbf and PANSS total scores are significant with p = 0.0272 and p = 0.0278 respectively.

To distinguish drug effect and disease effect in SZ group, we further explore the correlation between SZ-on and PANSS total, and between SZ-off and PANSS total. The interesting thing is only significant correlation was found between SZ-off and PANSS total, which manifests that PANSS total scores are more related to disease effect instead of drug effect. (Figure 20)

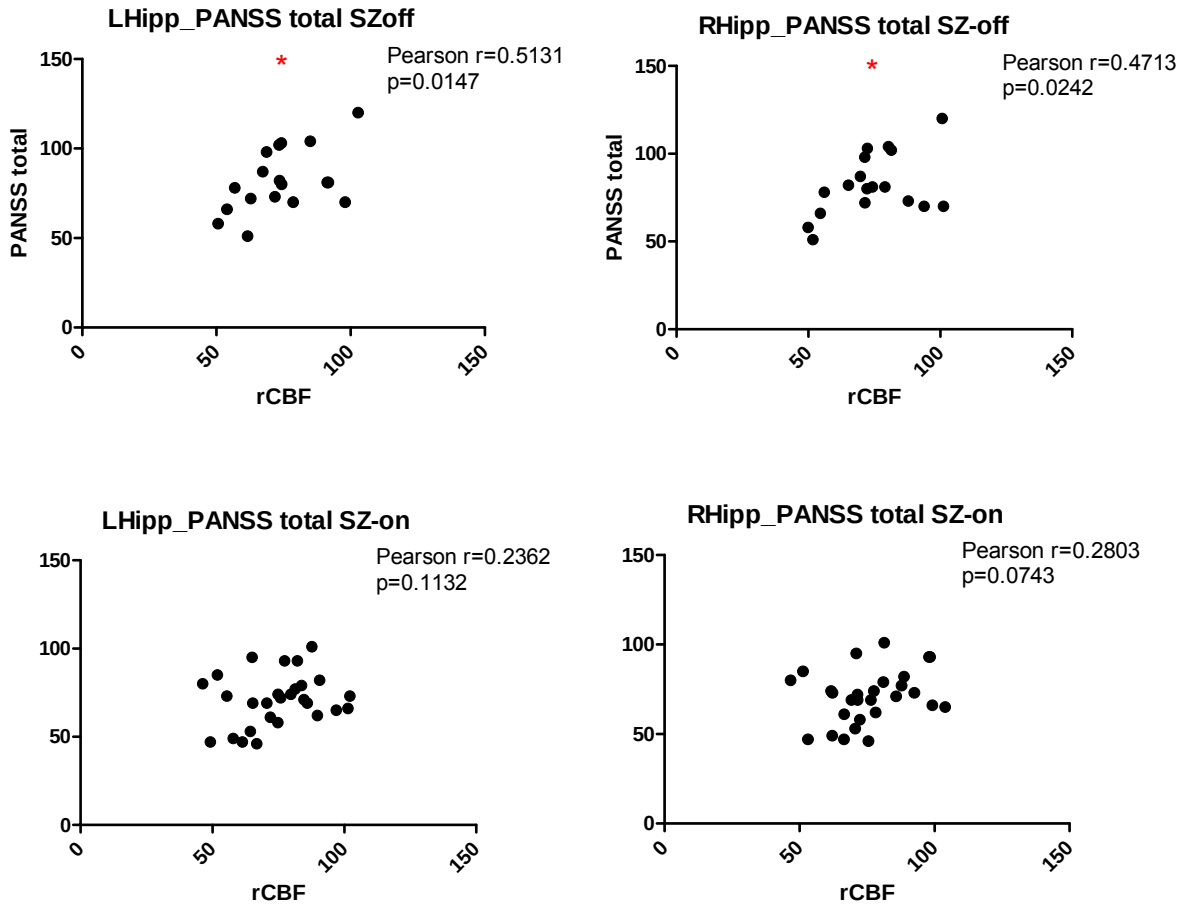

Fig 20. Correlation between PANSS total score and hippocampal rCBF in SZ-off and SZ-on.

Significant Pearson correlation was found between left and right hippocampal rCBF of SZ-off group and PANSS total scores (upper left and right), while no significant Pearson correlation was found between left and right hippocampal rCBF of SZ-on group and PANSS total scores (lower left and right).

Disscussion

Although no difference in hippocampal rCBF was detected between NC and SZ groups, which might be due to considerable variance among subjects and relatively small change in CBF with disease, the significant positive correlation between SZ rCBF and PANSS total scores may still suggest consistency with our hypothesis that CBF is increased in hippocampus in schizophrenia. The correlation difference between SZ-on and SZ-off groups indicates the possibility that drug effect may hamper the CBF increase caused by schizophrenia. As a supplement to the VASO study, this pCASL measurement provides an alternative way to measure baseline neuronal activity in whole brain. One way to magnify the group difference is to increase subject number in each group. In the future, with more subjects and more brain areas studied, we shall be able to find more intriguing results.

Acknowledgment: The high resolution VASO study was done by Carolyn Sacco, Yan Fang, Perry Mihalakos, Subroto Ghose, Jinsoo Uh, Hanzhang Lu, Anthony Wagner, Carol Tamminga. I was responsible for the VASO data analysis with Jinsoo Uh's help and Carolyn Sacco's assistance in ROI drawing and matching.

The pCASL study was done by Yan Fang, Carolyn Sacco, Perry Mihalakos, Peiying Liu, Hanzhang Lu, Carol Tamminga. I was responsible for the ASL data analysis with Peiying Liu's help. Both VASO and pCASL researches were funded by NIMH R01MH083957-01A2 (PI: Carol Tamminga, MD).

CHAPTER FOUR

Acquired Equivalence (AE) Task measurement using fMRI

Introduction

Declarative memory dysfunction is postulated to be a consequence of the molecular alteration in dentate gyrus in schizophrenia, a reflection of reduced transmission at NMDA receptor.[107] Psychosis is considered a distinct symptom domain in schizophrenia based on its unique disease course, often beginning before psychosis onset and lasting without improvement across disease years.[108] Cognitive dysfunction is similar in new and chronic schizophrenic patients[109-113], between adult-onset and adolescent-onset schizophrenia[114,115], and to certain degree, similar in family members[116-118] and in high-risk not-yet-ill persons[119]. But it has been shown to be distinct in schizophrenia compared with non-schizophrenia psychosis (e.g., BP-, dementia- or drug-induced)[120,121]. In addition, cognitive deficits show only small to moderate correlations with clinical state[122], no change with antipsychotic drug treatment or gender effects[123,124].

The nature of cognitive dysfunction has been extensively examined in schizophrenia. Persons with the illness present a wide range of cognitive disturbances often said to be basic to the illness; it is particularly in the areas of memory and attention that deficits appear most pronounced.[125,126] Cognitive deficits show diversity among schizophrenic individuals in severity, type and extent.[127-129] Declarative memory is one of the most reliably impaired functions in schizophrenia. Poor declarative memory performance has been associated with reductions in hippocampal volume and hippocampal (right anterior) activations during novelty.[130,131] Moreover, this decrement in memory function is exacerbated by the anticholinergic 'load' of APDs.[132] In persons at ultra-high-risk for developing psychosis, it is the verbal memory index (due to lower logical memory scores) that identified those who went on to develop psychosis[119]. It is also the

case that unaffected relatives, especially those relatives who have schizophrenia-spectrum disorder, show poorer memory performance than controls on a range of memory tests.[133] Working memory has also been extensively examined in schizophrenia. Alterations in its performance and performance correlations with abnormalities in prefrontal cortex function are consistently found in unmedicated as well as medicated schizophrenia patients.[134-136] Verbal and spatial working memory alterations are pervasive in the illness and correlate with many of the other cognitive alterations in the illness. Aspects of working memory impairment have been correlated with negative symptoms and the language aspects of formal thought disorder.[137]

We would argue based on our metaplasticity model, that aspects of psychosis and memory dysfunction in schizophrenia are both supported by alterations in hippocampal function, with the cognition-associated lesion involved in skewing hippocampal function towards psychosis by generating increases in environment-independent LTP. Our central aim is to distinguish how the encoding and retrieval of relational or conjunctive representations is altered in persons with schizophrenia when they are treated with APDs or not and how this alteration may interact with psychotic symptoms. Conjunctive representations are thought to separately code elements of an event, maintaining the compositionality of the elemental representations and organizing them in terms of their relations to one another[138]. Importantly, the compositional nature of conjunctions allows for reactivation of representations from partial input (pattern completion)[139,140], a process thought to underlie event recollection and the flexible use of relational memory. Given the architecture of the intra-hippocampal subfields, attention has focused on CA3 and its interactions with ERc and CA1. A leading hypothesis is that CA3 mechanisms are central to the formation of conjunctive memories, as well as to subsequent pattern completion that constitutes retrieval of these representations[139,140]. Encoding of conjunctive representations may critically depend on wide spread collateral connections within CA3, comprising a powerful associative learning mechanism that allows for the binding of co-

occurring event inputs distributed to multiple CA3 neurons. At retrieval, conjunctive representations may permit associative recognition, inferential reasoning, and recollection through pattern completion mechanisms that result in retrieval of an extended representation from partial input. Pattern completion may critically depend on mechanisms in CA3, CA1, and SUB, and on their interactions.

Acquired equivalence (AE) task

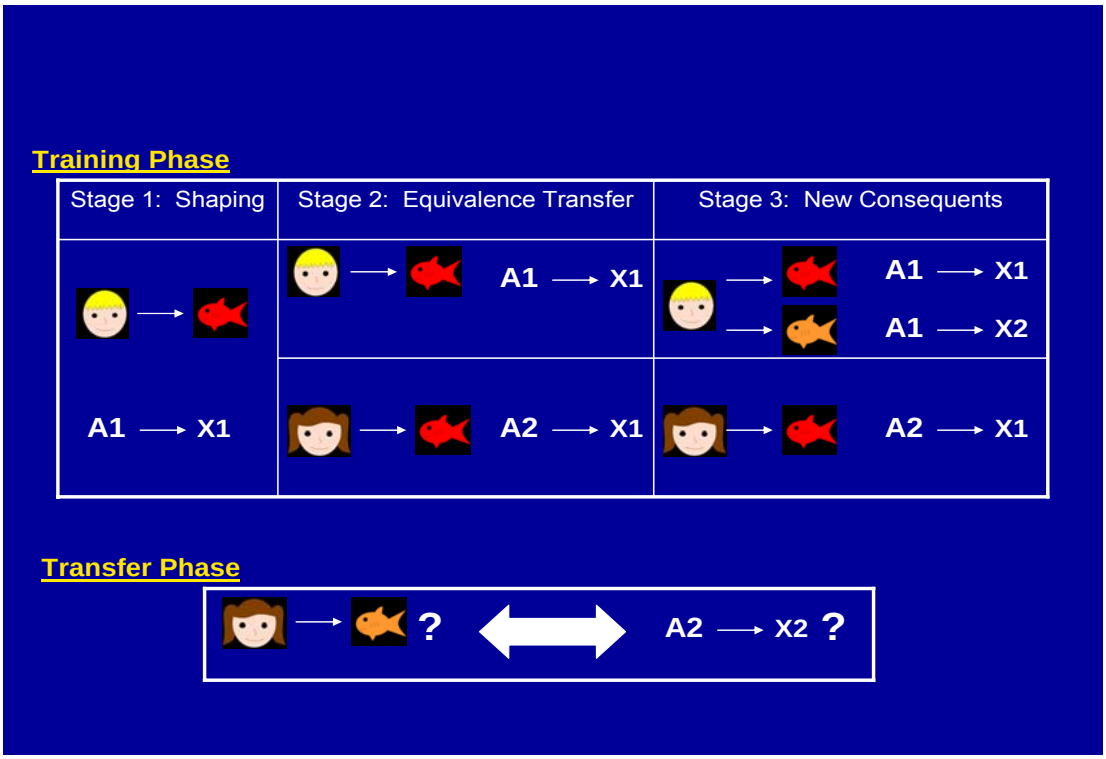

Fig 21. Demonstration of acquired Equivalence (AE) task with Training Phase (3 stages) and Transfer phase. Stage 1 and 2 in Training phase are finished outside the scanner. Stage 3 in Training phase and Transfer phase are finished inside the scanner.

Declarative memory supports the formation of flexibly addressable representations that enable inferences and generalizations about the world and self, and it is one of the most reliably

impaired functions in schizophrenia[142-144]. Transitive inferences depend on declarative memory for first order item-item relations as well as second order relations. The flexible nature of declarative memory processes in the MTL contrasts with the relatively inflexible stimulus-response or stimulus-stimulus associations that are incrementally acquired via basal ganglia learning mechanisms. In schizophrenia, evidence suggests that while basal ganglia functions are not grossly disturbed, hippocampal functions are disordered. Albeit, it is not all hippocampal functions which are disturbed but predominantly tasks which require inferential memory. The AE task is based on an initial learning phase, divided into three stages (see 'training phase' in figure 21) where volunteers gradually acquire associations between distinct stimuli (faces and fish) in a feedback paradigm, testing learning mechanisms. Subsequently, the subject is tested first on what they have explicitly learned ('trained") which examines recall and then subjects are tested on an ability to make an inference based on the learned data ("transfer') (see 'transfer phase' in figure 21). Since this task has been established, we are using this task to reveal the differences between function in normal and SZ volunteers. fMRI reveals that subsequent generalization is predicted by coupled activity in the hippocampus and midbrain dopamine regions during trial-by-error learning[147]. Next, because schizophrenia involves abnormalities in hippocampal and midbrain dopamine mechanisms and is treated using dopamine antagonist drugs, we test individuals with SZ on the same behavioral task, and examine the effect of medication on generalization performance.

Experimental method

'Trained' stages 1 and 2, with feed-back based stimulus-outcome learning, was conducted outside of the scanner prior to imaging. The stimulation tasks displayed on the screen subjects experienced throughout the experiment are presented in figure 22. Subjects had to achieve a performance criterion of 95% or better to proceed to the next phases. For stage 3, again feed-

back based stimulus-outcome learning was conducted, but within the MR scanner. Before the scan started, the following direction was shown on the screen, “Again you will see people and their pet fish. Different people have different kinds of fish. Now your job is to learn more about the kinds of fish each person has. You will need to remember what you have learned so far. When you have finished half of the trials, the computer will STOP SHOWING the correct answers. Keep making the best choices you can.” The total scan time for Stage 3 was 442.5 s x 2 runs, including 80 trials reinforcing all face/fish pairs from the AE training task (stages 1 and 2) and 40 trials introducing new consequences to be learned (stage 3), with a fixation crosshair interleaved. The stimulus time was 3 s, the feedback time was 2 s and the fixation crosshair time was 1.5 s. No performance criterion was required for stages 3 and transfer phase. After stage 3 was finished, the performance-test began seamlessly without new directions in the MR scanner. During the transfer phase, no feedback was provided and accuracy and reaction time collected as outcome measures. The total scan time for the transfer phase was 270 s x 2 runs, including 72 trials reinforcing all face/fish pairs from previous learning and 24 trials introducing transfer pairs. The stimulus time and the fixation crosshair time were the same as those in stage 3, and there was no feedback time in transfer phase.

All the scans were done in a whole-body 3T Philips Achieva scanner. A T1-weighted structural scan was obtained using 3D MPRAGE sequence with 160 1 mm slices and a 256 × 256 matrix. The in plane resolution of the MPRAGE image was 1mm × 1mm. The echo-planar imaging (EPI) fMRI scan was obtained with the parameters of TR 1500 ms, 30 sagittal slices, 5 mm slice thickness and 1 mm gap, FOV 192.5 × 220 × 179 mm^3, matrix 64 × 64, with resulting voxel dimension of 3.44 × 3.44 × 6 mm^3.

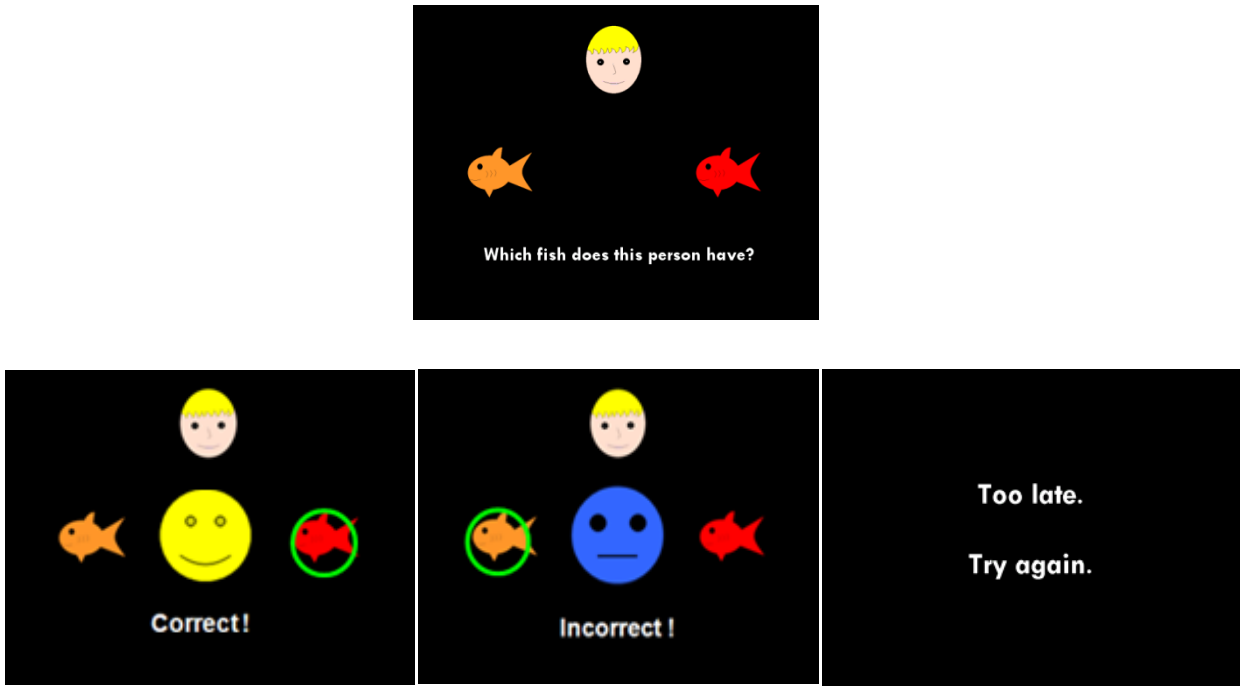

Fig 22. Stimulation AE tasks generated by E-Prime. One stimulation task displayed on the screen (upper image) and three distinctive feedbacks provided afterward according to subject's response. (lower images)

Data analysis

The AE data were all collected, with the images pre-processed in a group of N=19 normals, N=48 SZ (29 SZ-on and 19 SZ-off). Accuracy of responses was calculated in Excel by dividing the number of correct responses for each condition in each scan by the total number of responses for each condition. One NC subject and one SZ-on subject were excluded with their accuracy of responses below three standard deviation under group mean in the learning tasks. Table 4 is the demographic table. Significant difference in PANSS positive scores and PANSS total scores between SZ-on and SZ-off groups has been found. (Figure 23)

	age	gender	education	PANSS pos	PANSS total
NC	40±11	13M/5F	14±2		
SZ-on	42±10	19M/9F	12±3	19±5	71±15
SZ-off	37±10	13M/6F	13±3	23±6	82±17

Table 4. Demographic characteristics of all the volunteers in AE study.

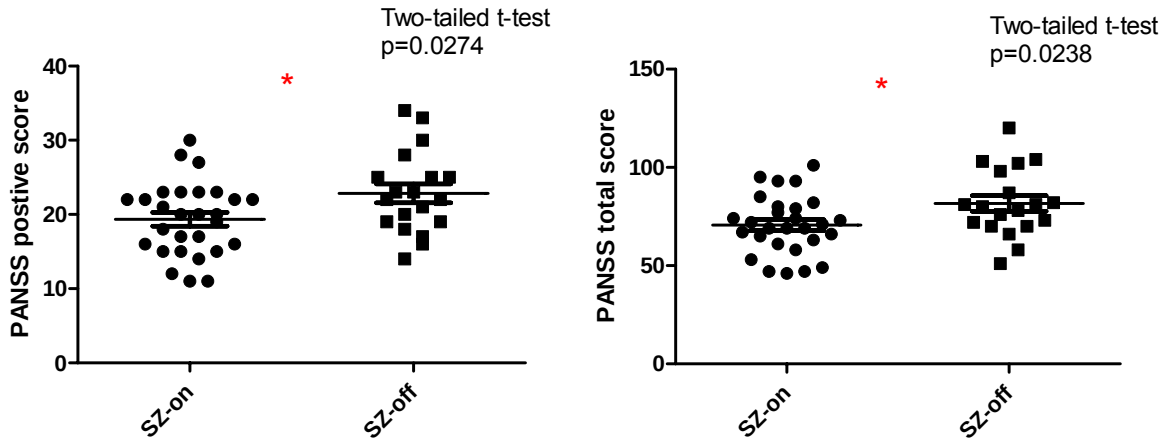

Fig 23. PANSS positive score distribution (left) and PANSS total score distribution (right) in SZ-on and SZ-off groups in AE study. PANSS pos and PANSS total are both significantly higher in SZ-off comparing to SZ-on.

Behavior results during both trained and transfer tasks are presented in figure 24. Although no significant difference was found between NC and SZ groups with Wilcoxon Mann Whitney non-parametric test, a tendency of decreased response accuracy is still clear in SZ group.

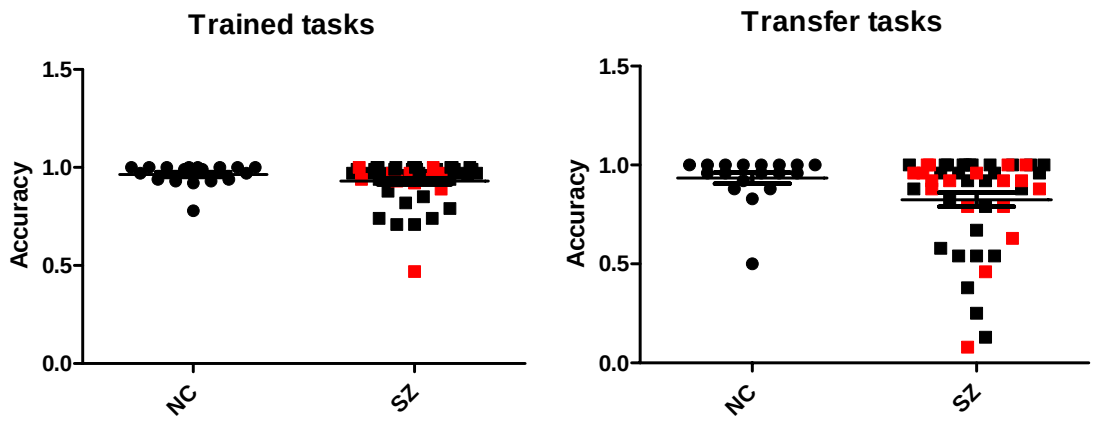

Fig 24. Behavior results of Trained and Transfer tasks in NC and SZ groups. SZ (SZ-on (black) and SZ-off (red)) Trained (93%; z=1.35, p=0.09) and Transfer (82%; z=1.56, p=0.06) accuracies are not significantly different from NC (92% and 96%, respectively) with Wilcoxon Mann Whitney non-parametric one-tailed test.

MRI images were converted to ANALYZE format and subsequent image processing was conducted using SPM5 running with Matlab 7.4.0 on a Linux platform. The EPI images were realigned first to correct for motion. The runs which had abrupt motion exceeding one voxel size were excluded from the analysis. The MPRAGE image was then coregistered to the mean of the realigned EPI images. The coregistered MPRAGE images were then normalized to the MNI brain template, and the same transfer parameters were used to normalize the EPI images. The normalized EPI images were resampled into 2 mm cubic voxels and smoothed with an 8mm full-width half-maximum Gaussian kernel to minimize effects of inter-subject anatomic variability. Time and dispersion derivatives of the hemodynamic function were included in the model to obtain a better fit to the data. A 128 second high-pass filter removed low-frequency noise and slow drifts in the signal. fMRI data were analyzed as an event-related design using the general linear model. In the single subject SPM models, responses to stimuli were modeled as events and convolved with the time-lagged canonical hemodynamic response function (default setting

in SPM) to account for the delay between event onset and expected increase of the blood oxygenation level-dependent (BOLD) signal. To account for variance caused by head movement, realignment parameters were included as additional regressors in the model. Flexible factorial design was used for the three-group (NC, SZ-on and SZ-off) and seven-condition (condition 1, 2, 3 in stage 3, and condition 1, 2, 3 and transfer in stage 4) analysis. Predicted activations were considered significant at $P < 0.05$ after correcting for False Discovery Rate (FDR) across the voxels.

ROI analysis uses three common ROI masks (left and right hippocampi, midbrain) generated from WFU PickAtlas (http://fmri.wfubmc.edu/software/PickAtlas) (Figure 25). For each ROI, the deconvolved signal was extracted for individual participants using a finite impulse response function implemented in MarsBaR (http://marsbar.sourceforge.net/). Integrated percent signal change was determined by calculating the area under the curve for the period of time 3-9 s post-stimulus onset for each condition.

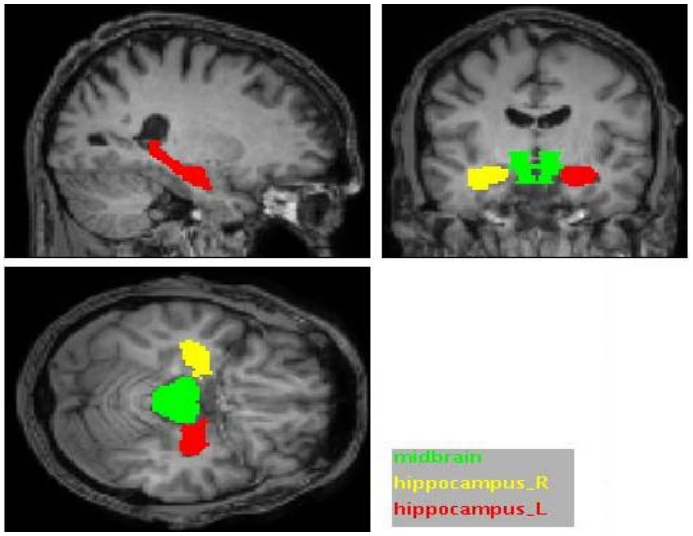

Fig 25. ROIs generated by WFU PickAtlas for AE ROI analysis. Three ROI masks (midbrain, right hippocampus, left hippocampus) overlay on one subject's anatomical brain image.

Result

According to our prediction and previous study, successful memory generalization is associated with coupled changes in learning-phase activity in the hippocampus and midbrain[147], and generalization is based on integrative encoding, whereby overlapping past events are integrated into a linked mnemonic representation. From Figure 26 we can see that the midbrain and posterior hippocampus are significantly activated during both trained and transfer tasks. In NC and SZ-off groups, the midbrain is more activated in the transfer tasks, but in SZ-on group, active regions in midbrain disminishes in the transfer tasks, consistent with the ROI analysis in midbrain in three groups and as predicted from the known effects of antipsychotic medications. The behavior data for the trained and transfer tasks in transfer phase also supports this finding although lacking statistical significance due to the large variance and small group difference. However, the hippocampus is only slightly activated in both tasks.

The comparison between NC and SZ groups of transfer tasks shows lower activation in the hippocampus, anterior and posterior cingulate gyrus, and medial prefrontal cortex in SZ compared to NC. During trained tasks, SZ shows lower activation in the basal ganglia and prefrontal cortex compared to NC. Correspondingly, the ROI measuremants in left hippocampus reveal reduced activity in SZ comparing to NC. (Figure 27)

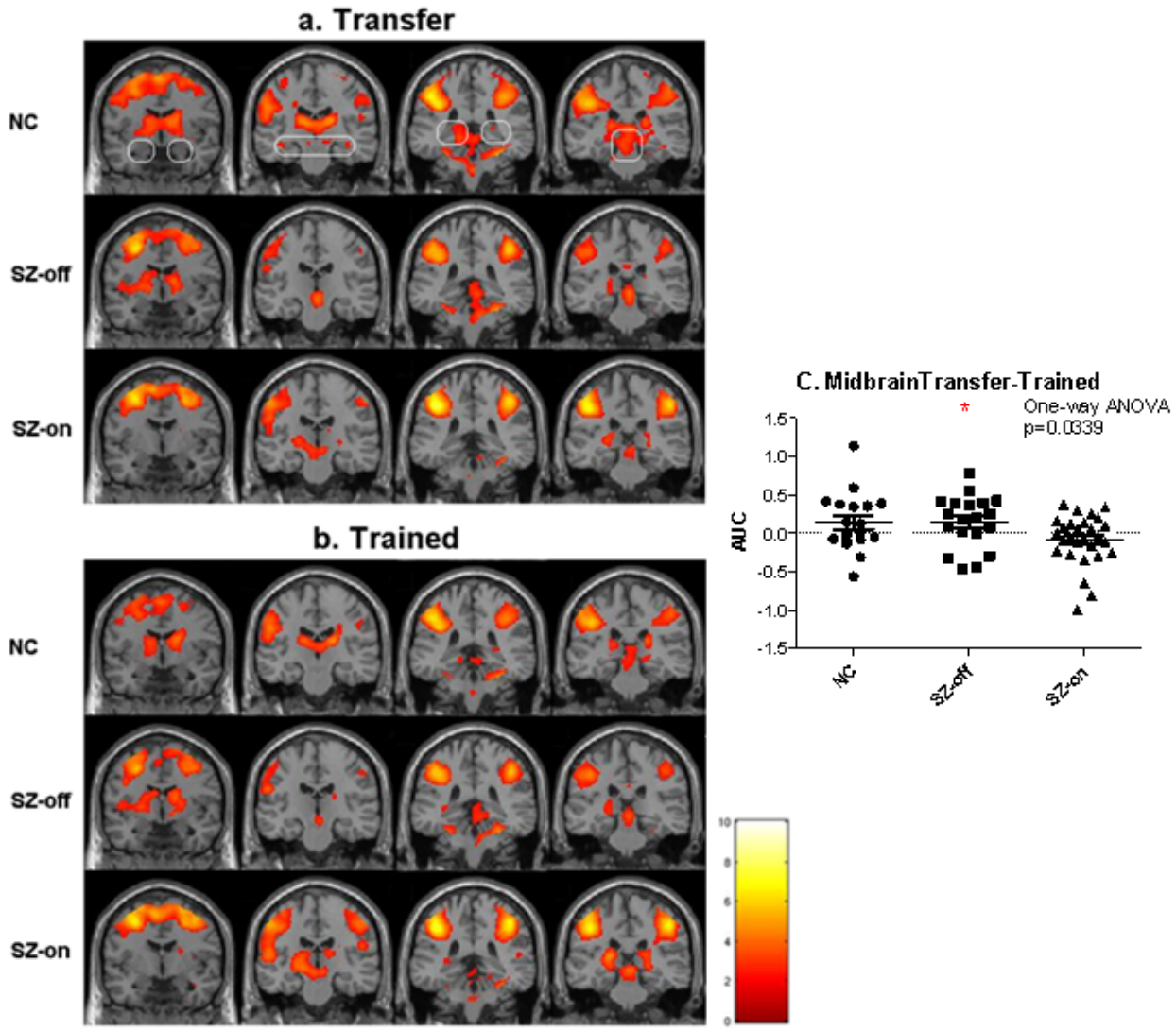

Fig 26. Within group AE fMRI and ROI results. During transfer phase, fMRI activity maps with p<0.05 (FDR corrected) and minimum cluster size of 5 voxels (K=5) for transfer tasks (a) and trained tasks (b) vs. baseline in NC, SZ-off and SZ-on groups. Area under the curve (AUC) measurements of HRF function for transfer-trained tasks in three groups show significant decrease in SZ-on group with one-way ANOVA analysis (p=0.0339). (c)

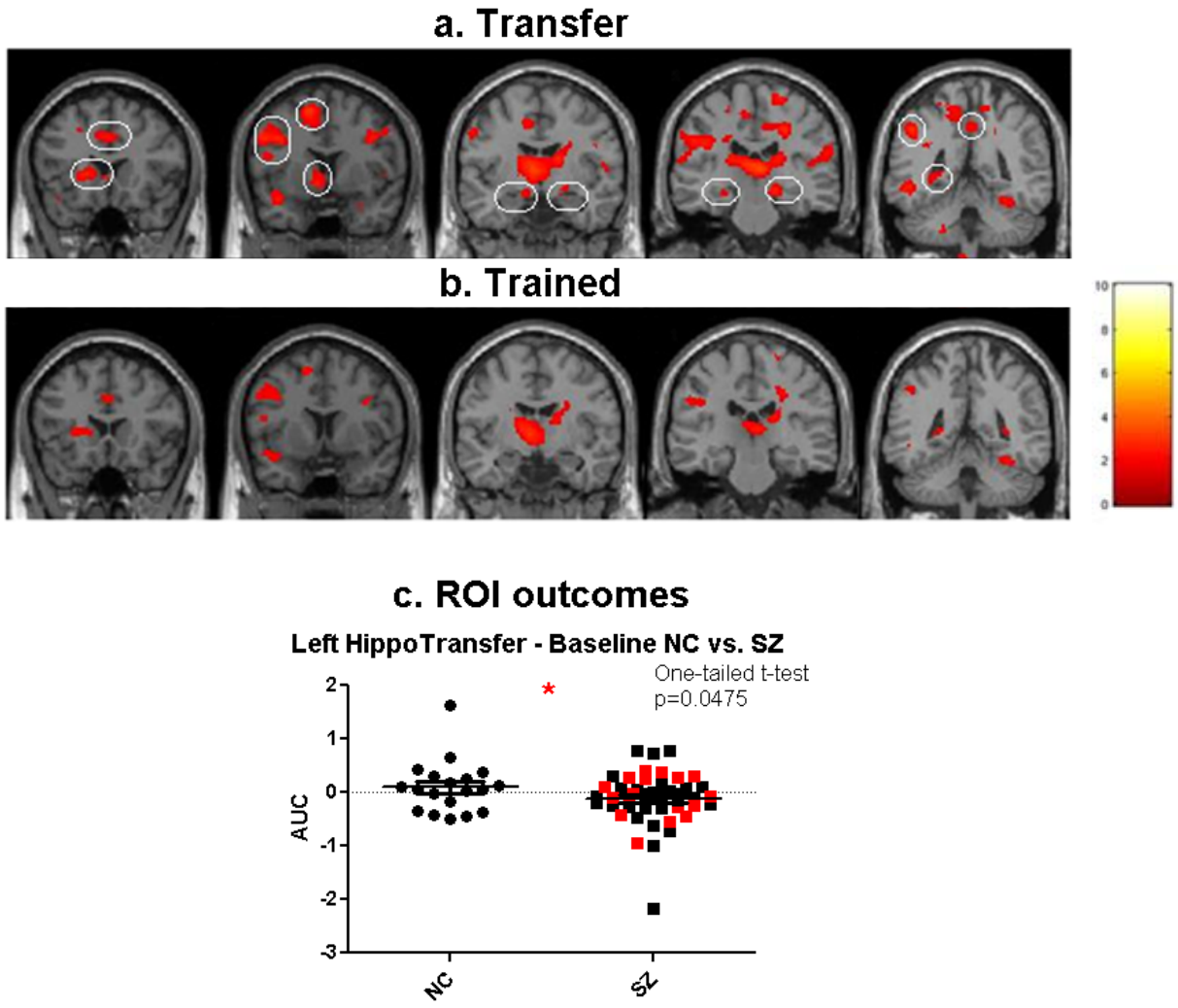

Fig 27. NC vs. SZ AE fMRI and ROI results. fMRI contrasts NC vs. SZ during transfer tasks (a) and trained tasks (b) with p<0.05 (uncorrected) and K=5. Area under the curve (AUC) measurements of transfer-baseline in NC and SZ groups (c) show significant decrease (p=0.0475) in SZ group comparing to NC group with one-tailed t-test.

To further explore difference between good and poor performers during transfer tasks, we divided the NC and SZ groups into good and poor subgroups by their median performance during transfer tasks. This resulted 8 good and 10 poor NC volunteers, 22 good (8 SZ-off, 14 SZ-on) and 25 poor (11 SZ-off, 14 SZ-on) SZ volunteers. The fMRI contrast result and behavior outcomes are presented in figure 28. From the activity maps we can see that brain activity

difference between NC/good and SZ/good is more related to posterior hippocampus, midbrain and neocortical regions, while brain activity difference between NC/poor and SZ/poor is apparent in anterior hippocampus and midbrain, which is also related to their behavior difference.

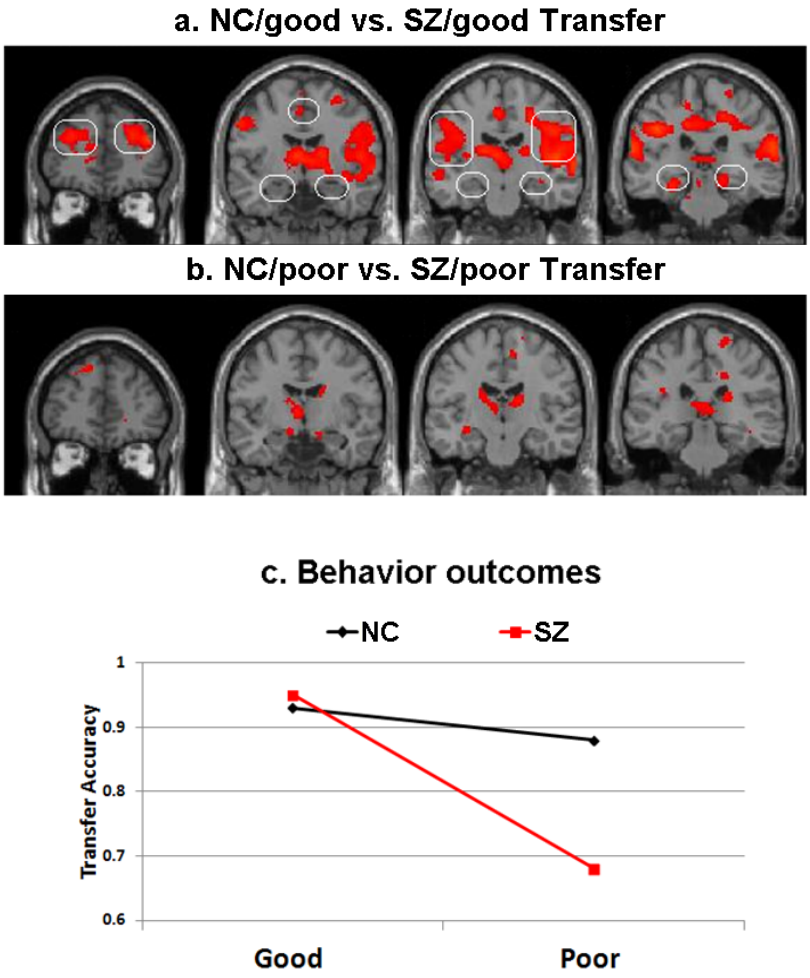

Fig 28. NC vs. SZ good and poor AE fMRI and behavior results. fMRI activity contrast maps in 'Good' (a) and 'Poor' (b) NC vs. SZ based on Transfer performance with $p<0.05$ (uncorrected) and $K=5$. Behavior outcomes of good and poor performers in NC and SZ (c) show SZ/Good has Transfer accuracy similar to NC/Good ($z=1.12$, $p=0.26$), while SZ/poor has lower Transfer accuracy compared to NC/poor ($z=2.76$, $p=0.006$) with Wilcoxon Mann Whitney two-tailed non-parametric test.

The difference between good and poor NC vs. SZ contrast maps may suggest that NC and SZ good and poor volunteers use different brain circuits to process the relational memory. To confirm our hypothesis, we also checked the within group activity maps of NC good/poor, SZ good/poor volunteers and the results are shown in figure 29. From these within group activity maps, we can see the good NC/SZ volunteers have anterior hippocampus activated, but the poor NC/SZ volunteers do not, although their contrast map shows a difference in anterior hippocampus. This is consistent with our hypothesis and former study that anterior hippocampus is closely related to subject performance during transfer tasks.[147] In addition, it's surprising to see the difference between NC/good vs. SZ/good and NC/poor vs. SZ/poor activity maps. This may indicate different brain circuits were involed in good and poor performances during Transfer tasks in NC and SZ groups. To test our hypothesis, we acquired NC/good, SZ/good, NC/poor and SZ/poor Transfer activity maps at the same statistical level. (Fig) It is reasonable to see the good NC/SZ Transfer maps have more hippocampal activity. The good NC groups has more brain activity in neocortical areas, while the poor SZ group has more brain activity in neocortical area and midbrain. This reveals us the variant brain curcuits used among different groups during relational memory.

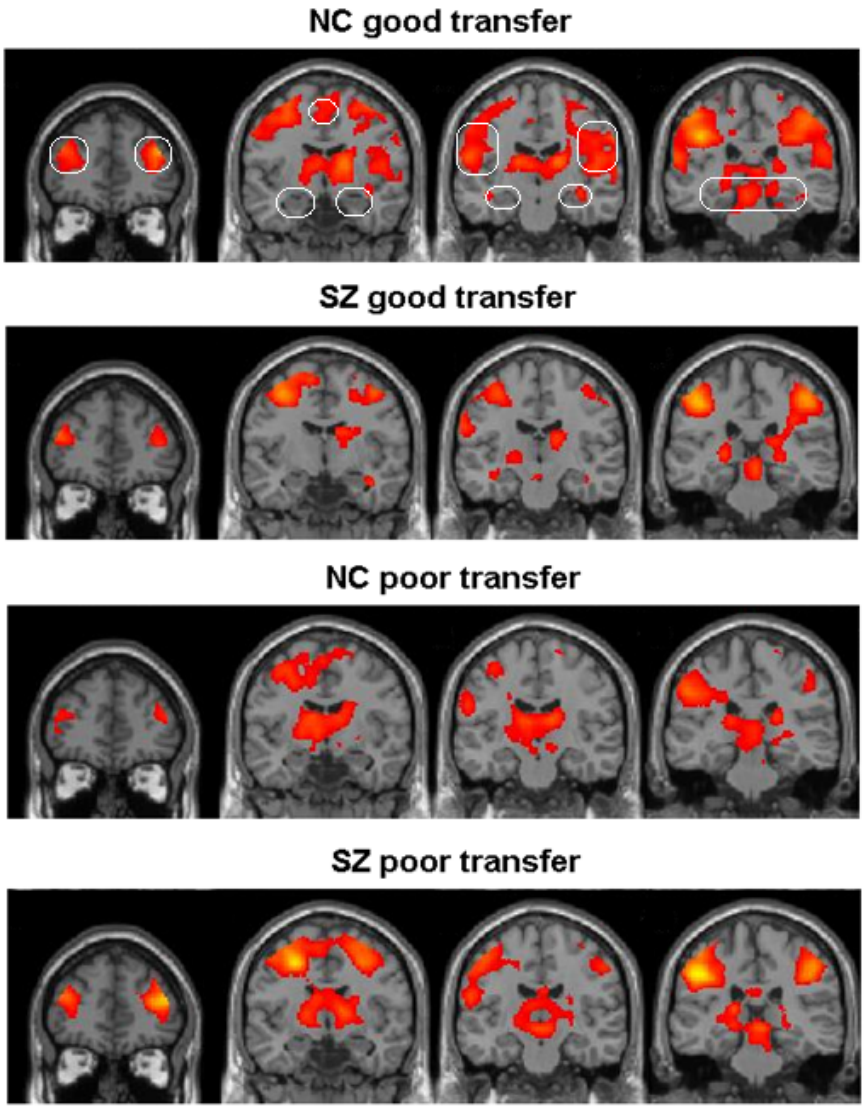

Fig 29. Within group good and poor AE Transfer fMRI results. NC/good, SZ/good, NC/poor and SZ/poor group Transfer activity maps with $p<0.05$ (uncorrected).

Discussion

Conform to our prediction, the midbrain is strongly activated during both training and transfer tasks. Through observation of the activity maps, in SZ-on group, the activated region in midbrain becomes smaller in the transfer task as compared to the training tasks, and during the transfer tasks, the hippocampus in NC groups is more activated than that in SZ-on and SZ-off groups,

these are consistent with our hypothesis that cerebral activations during relational memory performance are reduced in SZ, especially in those regions overlapping perfusion increases (CA3 and CA1 as measured with VASO), and that this reduction in neural activation is associated with the decrement in relational task performance, particularly in SZ-on where psychosis does not confound memory assessment. Here the NC vs. SZ-off contrast will give us an idea of disease effects, and the SZ-off vs. SZ-on will give us an idea of medication effect and the NC vs. SZ-on, an idea of residual memory load in the treated SZ state.

The behavioral outcomes show only a tendency for the SZ group to perform more poorly on response accuracy compared to NC, during both Transfer and Trained tasks; however, there are obviously a group of poor SZ performers. Therefore, we did a median split to examine the AE performance at the upper and lower ends during Transfer tasks. When contrasting 'Good' performers across NC and SZ volunteers, accuracies are similar; however, when contrasting 'Poor' performers across NC and SZ volunteers, the 'Poor' SZ performers are significantly worse on Transfer accuracy than the 'Poor' NC. It is when contrasting NC vs. SZ 'Good' performers that greater activation difference is obtained in hippocampus and neocortical regions. The exploration of NC and SZ 'Good' and 'Poor' Transfer activity individually suggests different brain circuits involved.

This study shows that limbic brain regions are dysfunctional during relational memory performance in SZ, including hippocampus, cingulate gyrus, and prefrontal cortex. During both AE Transfer and Trained tasks, hippocampal and midbrain activations are coupled. We suggest that these cerebral changes in schizophrenia are associated with increased baseline activity in hippocampus, and generate hyperactivity-induced inefficiency in memory processing.

The BOLD response is a sensitive indicator of where neural activity has acutely changed in response to a transient stimulus. However, the interpretation of altered responses in disease populations is intrinsically ambiguous. BOLD is sensitive to changes in deoxyhaemoglobin

levels, which are reduced during acute activation because cerebral blood flow (CBF) increases much more than the cerebral metabolic rate of oxygen ($CMRO_2$) consumption. Mathematical modeling of the BOLD response is complicated, and it turns out to be strongly modulated by two additional confounding factors that act independently on neural activity: baseline deoxyhaemoglobin level and the precise ratio of the fractional changes in CBF and $CMRO_2$. Both of these two factors are highly variable across different brain regions and in ageing and disease. Thus, when different BOLD responses are observed, they do not necessarily reflect differences in neural or metabolic activity. By contrast, fMRI measures of basal CBF or CBV often provide an accurate map of metabolic state.[141] Since we have found an increased basal neuronal activity in SZ group from our VASO study, this elevated baseline measurement can contribute to the reduced BOLD activity as measured in the AE fMRI task in SZ.

Acknowledgment: The AE study was done by Yan Fang, Carolyn Sacco, Perry Mihalakos, Hanzhang Lu, Anthony Wagner, Elena Ivleva, Carol Tamminga. I was responsible for the AE fMRI data analysis. This research is funded by NIMH R01MH083957-01A2 (PI: Carol Tamminga, MD).

CHAPTER FIVE

Conclusion

We generated several significant and interesting results with these imaging studies, some of which supported and some of which modified our original hypotheses. The high resolution VASO perfusion measures showed an increase in hippocampal subfields, specifically in CA3, CA1 and Subi, and the pCASL measures also showed positive correlation between disease effect and CBF in hippocampus, consistent with the hypothesis that basal neuronal activity is increased in these regions. The results of the AE fMRI BOLD imaging suggested that, with a declarative memory task, hippocampal activation is reduced in schizophrenia, an observation that is consistent with our hypothesis and the literature; we would suggest that this is due to an increased baseline firing or to a hyperactivity-induced inefficiency in memory processing. These results are consistent with our predictions from the metaplasticity model. The reduced glutamate relative concentrations in left hippocampus were predicted by our model and we interpret these as deriving from the putative NMDA receptor lesion in dentate gyrus in schizophrenia. The resultant reduction in glutamate signaling from DG to CA3 hypothetically provides an underlying molecular pathophysiology for the increase in CA3 sensitivity and hyperactivity, manifesting itself in the outcomes discussed above. That the hypoglutamatergic lesion in dentate gyrus would be sufficient to generate reduced hippocampal glutamate detected by MRS is demonstrated in our NR1-KO mouse study. These outcomes support the idea that increasing the basal neuronal activity in CA3 and CA1, decreases the efficiency of the pattern completion functions within CA3, resulting in hyperassociative memory, mistakes of memory and memories laid down with psychotic content. Due to limited sample sizes, some of our statistical analyses lack significance. These outcomes will have to be re-evaluated with increased subject number

and even more novel tasks for memory testing. Also, with a broad age range of the subjects and variable subject characteristics, these variables, if different between groups, can confound our examination of schizophrenia pathophysiology, especially in the high resolutions studies.

BIBLIOGRAPHY

1. Kandel ER, Schwartz JH, Jessell TM. (2000) Principles of neuroscience. Fourth edition.
2. Tamminga CA, Holcomb HH. (2004) Phenotype of schizophrenia: a review and formulation. Mol. Psychiatry 10:27-39.
3. Carpenter WT Jr, Buchanan, RW. (1994) Schizophrenia. N. Engl. F. Med. 330:681-690.
4. Sartorius N, Shapiro R, Jablensky A. (1974) The International Pilot Study of Schizophrenia. Schizophr. Bull 1:21-34.
5. Davis R, Whittington R, Bryson HM. (1997) Nefazodone: a review of its pharmacology and clinical efficacy in the management of major depression. Drugs 53:608-636.
6. Awad AG, Voruganti LN. (2008) The burden of schizophrenia on caregivers: a review. Pharmacoeconomics 26:149-162.
7. Tamminga CA, Davis JM. (2007) The neuropharmacology of psychosis. Schizophr. Bull 33:937-946.
8. Davis JM. (1969) Review of antipsychotic drug literature. In Diagnosis and Drug Treatment of Psychiatric Disorders, ed. DF Klein, JM Davis, pp. 52-138. Baltimore, MD: The Williams and Wilkins Company.
9. American Psychiatric Association. (2000) Diagnostic and Statistical Manual of Mental Disorders, Fourth Edition Text Revision (DSM-IV-TR). Washington, DC: Am. Psychiatr. Assoc.
10. Harvey PD, Howanitz E, Parrella M, White L, Davidson M, Mohs RC, Hoblyn J, Davis KL. (1998) Symptoms, cognitive functioning, and adaptive skills in geriatric patients with lifelong schizophrenia: a comparison across treatment sites. Am. J. Psychiatry 155(8):1080-86.
11. Leucht S, Kissling W, Davis JM. (2009) Second-generation antipsychotics for schizophrenia: Can we resolve the conflict? Psychol. Med. 39:1591-1602.
12. Leucht S, Wahlbeck K, Hamann J, Kissling W. (2003) New generation antipsychotics versus low-potency conventional antipsychotics: a systematic review and meta-analysis. Lancet 361:1581-1589; comment 362:404, author reply 404-405.

13. Flashman LA, Green MF. (2004) Review of cognition and brain structure in schizophrenia: profiles, longitudinal course, and effects of treatment. Psychiatr. Clin. North Am. 27:1-18, vii.
14. Cornblatt BA, Erlenmeyer-Kimling L. (1985) Global attentional deviance as a marker of risk for schizophrenia: specificity and predictive validity. J. Abnorm. Psychol 94:470-486.
15. Ibrahim HM, Tamminga CA. (2011) Schizophrenia: treatment targets beyond monoamine systems. Annu. Rev. Pharmacol. Toxicol. 51:189-209.
16. Censits DM, Ragland JD, Gur RC, Gur RE. (1997) Neuropsychological evidence supporting a neurodevelopmental model of schizophrenia: a longitudianl study. Schizophr. Res. 24:289-98.
17. Goldberg TE, Weinberger DR. (1996) Effects of neuroleptic medications on the cognitions of patients with schizophrenia: a review of recent studies. J. Clin. Psychiatry 57:62-65.
18. Marder SR. (2006) The NIMH-MATRICS project for developing cognition-enhancing agents for schizophrenia. Dialogues Clin, Neurosci. 8:109-13.
19. Geyer MA, Tamminga C. (2004) MATRICS: Measurement and Treatment Research to Improve Cognition in Schizophrenia. Psychopharmacology 174:1-162.
20. Green MF, Olivier B, Crawley JN, Penn DL, Silverstein S. (2005) Social cognition in schizophrenia: recommendations from the Measurement and Treatment Research to Improve Cognition in Schizophrenia New Approaches Conference. Schizophr. Bull. 31:882-887.
21. Golgi C. (1873) Sulla struttura della sostanza grigia dell cervello. Gazz Med Lombarda 33:244-246.
22. Ramo´n y Cajal S. (1909) Histologie du syste`me nerveux de l' homme et des verte´bre´s. Tome I. Paris: Malone.
23. Ramo´n y Cajal S. (1911) Histologie du syste`me nerveux de l' homme et des verte´bre´s. Tome II. Paris: Malone.
24. Ramo´n y Cajal S, Azoulay L. (1894) Les nouvelles ide´es sur la structure du syste`me nerveux chez l'homme et chez les verte´bre´s Paris: C. Reinwald.
25. Zille K. Amunts K. (2010) Centenary of Brodmann's map-conception and fate. Nat Rev Neurosci 11:139-145.

26. Brodmann K. (1909) Vergleichende Lokalisationslehre der Grosshirn-rinde in ihren Prinzipien dargestellt auf Grund des Zellenbaues. Leipzig: JA Barth. x, 324 p.
27. Port JD, Agarwal N. (2011) MR Spectroscopy in Schizophrenia. Journal of MRI. 34: 1251-1261.
28. Mountcastle VB. (1957) Modality and topographic properties of single neurons of cat's somatic sensory cortex. J Neurophysiol 20:408-434.
29. Grinvald A, Slovin H, Vanzetta I. (2000) Non-invasive visualization of cortical columns by fMRI. Nat Neurosci 3:105-107.
30. Kantrowitz JT, Javitt DC. (2010) N-methyl-D-aspartate (NMDA) receptor dysfunction or dysregulation: The final common pathway on the road to schizophrenia?. Brain Res. Bull. 83:108-121.
31. Debanne D, Daoudal G, Sourdet V, Russier M. (2003) Brain plasticity and ion channels. J. Physiol. Paris 97(4–6):403–414.
32. Pérez-Otaño I, Ehlers MD. (2005) Homeostatic plasticity and NMDA receptor trafficking. Trends Neurosci. 28(5):229–238.
33. Asztély F, Gustafsson B. (1996) Ionotropic glutamate receptors. Their possible role in the expression of hippocampal synaptic plasticity. Mol. Neurobiol. 12(1):1–11.
34. Weiler IJ, Greenough WT. (1993) Metabotropic glutamate receptors trigger postsynaptic protein synthesis. Proc. Natl. Acad. Sci. U.S.A. 90(15):7168–7171.
35. Petroff OA. (2002) GABA and glutamate in the human brain. Neuroscientist 8(6):562–573.
36. Schousboe A, Waagepetersen HS. (2007) GABA: homeostatic and pharmacological aspects. Prog. Brain Res. Progress in Brain Research 160:9–19.
37. Bear MF, Connors BW, Paradiso MA. (2007) Neuroscience Exploring the brain. Third edition.
38. Lodge DJ, Grace AA. (2011) Hippocampal dysregulation of dopamine system function and the pathophysiology of schizophrenia. Trends in Pharmacological Sciences 32:507-513.
39. Tamminga CA, Stan AD, Wagner AD. (2010) The hippocampal formation in schizophrenia. Am J Psychiatry 167(20):1178-1193.
40. Cohen N, Eichenbaum H. (1993) Memory, Amnesia, and the Hippocampal System. Cambridge, Mass, MIT Press.

41. McClelland JL, McNaughton BL, O'Reilly RC. (1995) Why there are complementary learning systems in the hippocampus and neocortex: insights from the success and failure of connectionist models of learning and memory. Psychol Rev. 102:419-457.
42. Norman KA, O'Reilly RC. (2003) Modeling hippocampal and neocortical contributions to recognition memeory: a complementary-learning-systems approach. Psychol Rev. 110:611-646.
43. Bontempi B, Laurent-Demir C, Destrade C, Jaffard R. (1999) Time-dependent reorganization of brain circuitry underlying longterm memory storage. Nature. 400:671-675.
44. Marr D. (1971) Simple memory: a theory for archicortex. Philos Trans R Soc Lond B Biol Sci. 262: 23-81.
45. Zola-Morgan S, Squire LR. (1993) Neuroanatomy of memory. Annu Rev Neurosci. 16:547-563.
46. Fanselow MS, Dong HW (2010) "Are the dorsal and ventral hippocampus functionally distinct structures?" Neuron. 65:7-19.
47. Best T, Wilson IA, Witter MP, Morris RG. (2009) From rapid place learning to behavioral performance: a key role for the intermediate hippocampus. PLoS Biol. 7, e 1000089
48. Bast T, Feldon J. (2003) Hippocampal modulation of sensorimotor processes. Prog. Neurobiol. 70:319-345.
49. Moser MB, Moser EI. (1998) Functional differentiation in the hippocampus. Hippocampus 8:608-619.
50. Lau JY, Goldman D, Buzas B, Hodgkinson C, Leibenluft E, Nelson E, Sankin L, Pine DS, Ernst M. (2010) BDNF gene polymorphism [Val66Met] predicts amygdala and anterior hippocampus responses to emotional faces in anxious and depressed adolescents. Neuroimage 53:952-961.
51. Casanova MF, Rothberg B. (2002) Shape distortion of the hippocampus: a possible explanation of the pyramical cell disarray reported in schizophrenia. Schzophr. Res. 55: 19-24.
52. Narr KL, Thompson PM, Szeszko P, Robinson D, Jang S, Woods RP, Kim S, Hayashi KM, Asunction D, Toga AW, Bilder RM. (2004) Regional specificity of hippocampal volume reductions in first-episode schizophrenia. Neuroimage 21:1563-1575.

53. Weiss AP, Schacter DL, Goff DC, Rauch SL, Alpert NM, Fischman AJ, Heckers S. (2003) Impaired hippocampal recruitment during normal modulation of memory performance in schizophrenia. Biol. Psychiatry 53:48-55.
54. Heckers S, Rauch SL, Goff D, Savage CR, Schacter DL, Fischman AJ, Alpert NM. (1998) Impaired recruitment of the hippocampus during conscious recollection in schizophrenia. Nat. Neurosci. 1:318-323.
55. Harrison PJ. (1999) The neuropathology of schizophrenia. A critical review of the data and their interpretation. Brain 122 (Pt 4):593-624.
56. Heckers S and Konradi C. (2002) Hippocampal neurons in schizophrenia. J. Neural Transm. 109:891-905.
57. Nelson MD, Saykin AJ, Flashman LA, Riordan HJ. (1998) Hippocampal volume reduction in schizophrenia as assessed by magnetic resonance imaging: a meta-analytic study. Arch. Gen. Psychiatry 55:433-440.
58. Medoff DR, Holcomb HH, Lahti AC, Tamminga CA. (2001) Probing the human hippocampus using rCBF: contrasts in schizophrenia. Hippocampus 11:543-550.
59. Schobel SA, Lewandowski NM, Corcoran CM, Moore H, Brown T, Malaspina D, Small SA. (2009) Differential targeting of the CA1 subfield of the hippocampal formation by schizophrenia and related psychotic disorders. Arch Gen Psychiatry 66(9):938-946.
60. Molina V, Reig S, Sarramea F, Sanz J, Francisco Artaloytia J, Luque R, Aragüés M, Pascau J, Benito C, Palomo T, Desco M. (2003) Anatomical and functional cerebral variables associated with basal symptoms but not risperidone response in minimally treated schizophrenia. Psychiatry Res. – Neuroimaging 124:163-175.
61. Bienenstock EL, Cooper LN, Munro PW. (1982) Theory for the development of neuron selectivity: orientation specificity and binocular interaction in visual cortex. J Neurosci. 2(1):32-48.
62. Bear MF. (2003) Bidirectional synaptic plasticity: from theory to reality. Philos Trans R Soc Lond B Biol Sci. 358(1432):649-655.
63. Tsai G, Coyle JT. (2002) Glutamatergic mechanisms in schizophrenia. Annu Rev Pharmacol

Toxicol. 42:165-179.

64. Tamminga CA. Schizophrenia and glutamatergic transmission. Critical Reviews in Neuroscience 1996.
65. Harrison PJ. (2004) The hippocampus in schizophrenia: a review of the neuropathological evidence and its pathophysiological implications. Psychopharmacology 174(1):151-162.
66. Lau CG, Zukin RS. (2007) NMDA receptor trafficking in synaptic plasticity and neuropsychiatric disorders. Nat Rev Neurosci 8(6):413-426.
67. Gao XM, Sakai K, Roberts RC, Conley RR, Dean B, Tamminga CA. (2000) Ionotropic glutamate receptors and expression of N-methyl-D-aspartate receptor subunits in subregions of human hippocampus: effects of schizophrenia. Am J Psychiatry 157(7):1141-1149.
68. Altar CA, Jurata LW, Charles V, Lemire A, Liu P, Bukhman Y, Yong TA, Bullard J, Yokoe H, Webster MJ, Knable MB, Brockman JA. (2005) Deficient hippocampal neuron expression of proteasome, ubiquitin, and mitochondrial genes in multiple schizophrenia cohorts. Biol Psychiatry 58(2):85-96.
69. Ghose S, Gao XM, Stan AD et al. Toward an Anatomy of Glutamate Dysfunction in Schizophrenia: a Focus on the Medial Temporal Lobe. 2007.
70. Abraham WC, Bear MF. Metaplasticity: the plasticity of synaptic plasticity. (1996) Trends Neurosci 19(4):126-130.
71. Malenka RC, Bear MF. (2004) LTP and LTD: an embarrassment of riches. Neuron 44(1):5-21.
72. Philpot BD, Cho KK, Bear MF. (2007) Obligatory Role of NR2A for Metaplasticity in Visual Cortex. Neuron 53(4):495-502.
73. Chen WS, Bear MF. (2007) Activity-dependent regulation of NR2B translation contributes to metaplasticity in mouse visual cortex. Neuropharmacology 52(1):200-214.
74. Iny K, Heynen AJ, Sklar E, Bear MF. (2006) Bidirectional modifications of visual acuity induced by monocular deprivation in juvenile and adult rats. J Neurosci 26(28):7368-7374.
75. Marder CP, Buonomano DV. (2003) Differential effects of short- and long-term potentiation on cell firing in the CA1 region of the hippocampus. J Neurosci 23(1):112-121.

76. Sacco C, Fang Y, Mihalakos P, Uh J, Lu H, Wagner A, Tamminga C. (2010) UT Southwestern Medical Center AIRC retreat poster.
77. Bogerts B, Ashtari M, Degreef G, Alvir JM, Bilder RM, Lieberman JA. (1990) Reduced temporal limbic structure volumes on magnetic resonance images in first episode schizophrenia. Psychiatry Res 35(1):1-13.
78. Heckers S. (2001) Neuroimaging studies of the hippocampus in schizophrenia. Hippocampus 11(5):520-528.
79. Gao XM, Sakai K, Roberts RC, Conley RR, Dean B, and Tamminga CA. (2000) Ionotropic glutamate receptors and expression of N-methyl-D-aspartate receptor subunits in subregions of human hippocampus: effects of schizophrenia. Am J Psychiatry 157:1141-1149.
80. Ghose S, Chin R, Gallegos A, Roberts R, Coyle J, and Tamminga C. (2009) Localization of NAAG-related gene expression deficits to the anterior hippocampus in schizophrenia. Schizophr Res 111:131-137.
81. Heckers S, Stone D, Walsh J, Shick J, Koul P, and Benes FM. (2002) Differential hippocampal expression of glutamic acid decarboxylase 65 and 67 messenger RNA in bipolar disorder and schizophrenia. Arch Gen Psychiatry 59:521-529.
82. Steen RG, Hamer RM, Lieberman JA. (2005) Measurement of brain metabolites by 1H magnetic resonance spectroscopy in patients with schizophrenia: a systematic review and meta-analysis. Neuropsychopharmacology. 30(11):1949-1962.
83. First MB, Spitzer RL, Gibbon M, Williams JBW. (2002) Structured Clinical Interview for DSM-IV-TR Axis I Disorders, Research Version, Patient Edition. (SCID-I/P) New York: Biometrics Research, New York State Psychiatric Institute.
84. Kay SR, Fiszbein A, and Opler LA. (1987) The positive and negative syndrome scale (PANSS) for schizophrenia. Schizophr Bull 13:261-276.
85. Mescher M, Merkle H, Kirsch J, Garwood M, and Gruetter R. (1998) Simultaneous in vivo spectral editing and water suppression. NMR Biomed 11:266-272.
86. Provencher SW. (1993) Estimation of metabolite concentrations from localized in vivo proton NMR spectra. Magn Reson Med 30(6):672-679.

87. Provencher SW. (2001). Automatic quantitation of localized in vivo 1H spectra with LCModel. NMR Biomed 14:260-264.
88. Gruetter R, Weisdorf SA, Rajanayagan V, Terpstra M, Merkle H, Truwit CL, Garwood M, Nyberg SL, Ugurbil K. (1998) Resolution improvements in in vivo ^{1}H NMR spectra with increased magnetic field strength. J Magn Reson 135:260-264.
89. van Elst LT, Valerius G, Buchert M, Thiel T, Rusch N, Bubl E, Hennig J, Ebert D, and Olbrich HM. (2005) Increased prefrontal and hippocampal glutamate concentration in schizophrenia: evidence from a magnetic resonance spectroscopy study. Biol Psychiatry 58:724-730.
90. Lutkenhoff ES, van Erp TG, Thomas MA, Therman S, Manninen M, Huttunen MO, Kaprio J, Lonnqvist J, O'Neill J, and Cannon TD. (2010) Proton MRS in twin pairs discordant for schizophrenia. Mol Psychiatry 15(3):308-318.
91. Stone JM, Day F, Tsagaraki H, Valli I, McLean MA, Lythgoe DJ, O'Gorman RL, Barker GJ, and McGuire PK. (2009) Glutamate dysfunction in people with prodromal symptoms of psychosis: relationship to gray matter volume. Biol Psychiatry 66:533-539.
92. Olbrich HM, Valerius G, Rusch N, Buchert M, Thiel T, Hennig J, Ebert D, and Van Elst LT. (2008) Frontolimbic glutamate alterations in first episode schizophrenia: evidence from a magnetic resonance spectroscopy study. World J Biol Psychiatry 9:59-63.
93. Patel AB, De Graaf RA, Mason GF, Rothman DL, Shulman RG, and Behar KL. (2003) Coupling of glutamatergic neurotransmission and neuronal glucose oxidation over the entire range of cerebral cortex activity. Ann N Y Acad Sci 1003:452-453.
94. Rothman DL, Behar KL, Hyder F, and Shulman RG. (2003) In vivo NMR studies of the glutamate neurotransmitter flux and neuroenergetics: implications for brain function. Annu Rev Physiol 65:401-427.
95. Duvernoy HM, and Bourgouin P. (1998) The human hippocampus : functional anatomy, vascularization and serial sections with MRI, 2nd completely rev. and expanded edn (Berlin ; New York, Springer).
96. Lavenex P, and Amaral DG. (2000) Hippocampal-neocortical interaction: a hierarchy of associativity. Hippocampus 10:420-430.

97. Moffett JR, Ross B, Arun P, Madhavarao CN, and Namboodiri AM. (2007) N-Acetylaspartate in the CNS: from neurodiagnostics to neurobiology. Prog Neurobiol 81:89-131.

98. Steen RG, Hamer RM, and Lieberman JA. (2005) Measurement of brain metabolites by 1H magnetic resonance spectroscopy in patients with schizophrenia: a systematic review and meta-analysis. Neuropsychopharmacology 30:1949-1962.

99. Ongur D, Prescot AP, Jensen JE, Cohen BM, Renshaw PF. (2009) Creatine abnormalities in schizophrenia and bipolar disorder. Psychiatry Res 172:44-48.

100. Yoo SY, Yeon S, Choi CH, Kang DH, Lee JM, Shin NY, Jung WH, Choi JS, Jang DP, Kwon JS. (2009) Proton magnetic resonance spectroscopy in subjects with high genetic risk of schizophrenia: investigation of anterior cingulate, dorsolateral prefrontal cortex and thalamus. Schizphr Res 111:86-93.

101. Gruetter R, Weisdorf SA, Rajanayagan V, Terpstra M, Merkle H, Truwit CL, Garwood M, Nyberg SL, Ugurbil K. (1998) Resolution improvements in in vivo ^{1}H NMR spectra with increased magnetic field strength. J Magn Reson 135:260-264.

102. Choi C, Dimitrov IE, Douglas D, Patel A, Kaiser LG, Amezcua CA, Maher EA. (2010) Improvement of resolution for brain coupled metabolites by optimized ^{1}H MRS at 7T. NMR Biomed 23(9):1044-1052.

103. Rosen BR, Belliveau JW, Vevea JM, Brady TJ. (1990) Perfusion imaging with NMR contrast agents. Magn Reson Med 14:249-265.

104. Lu H, Law M, Johnson G, Ge Y, van Zijl PC, and Helpern JA. (2005) Novel Approach to Measure Absolute Cerebral Blood Volume using Vascular-Space-Occupancy (VASO) Dependent MRI. Magnetic Resonance in Medicine 54:1403-1411.

105. Malaspina D, Harkavy-Friedman J, Corcoran C, Mujica-Parodi L, Printz D, Gorman JM, Van Heertum R. (2004) Resting neural activity distinguishes subgroups of schizophrenia patients. Biol Psychiatry 56(12):931–937.

106. Kawasaki Y, Suzuki M, Maeda Y, Urata K, Yamaguchi N, Matsuda H, Hisada K, Suzuki M, Takashima T. (1992) Regional cerebral blood flow in patients with schizophrenia. Eur Arch Psychiatry Clin Neurosci 241(4):195–200.

107. Coyle JT, Tsai G. (2004) The NMDA receptor glycine modulatory site: a therapeutic target for improving cognition and reducing negative symptoms in schizophrenia. Psychopharmacology (Berl) 174(1):32-38.

108. Cornblatt BA, Erlenmeyer-Kimling L. (1985) Global attentional deviance as a marker of risk for schizophrenia: specificity and predictive validity. Journal of Abnormal Psychology 94(4):470-486.

109. Bilder RM, Lipschutz-Broch L, Reiter G, Geisler S, Mayerhoff D, Lieberman JA. (1991) Neuropsychological deficits in the early course of first episode schizophrenia. Schizophr Res 5(3):198-199.

110. Gur RE, Turetsky BI, Bilker WB, Gur RC. (1999) Reduced gray matter volume in schizophrenia. Arch Gen Psychiatry 56(10):905-911.

111. Gur RE, Maany V, Mozley PD, Swanson C, Bilker W, Gur RC. (1998) Subcortical MRI Volumes in Neuroleptic- Naive and Treated Patients With Schizophrenia. Am J Psychiatry 155(12):1711-1717.

112. Hill SK, Beers SR, Kmiec JA, Keshavan MS, Sweeney JA. (2004) Impairment of verbal memory and learning in antipsychotic-naive patients with first-episode schizophrenia. Schizophr Res 68:127-136.

113. Saykin AJ, Shtasel DL, Gur RE, Kester DB, Mozley LH, Stafiniak P and Gur RC. (1994) Neuropsychological deficits in neuroleptic naive patients with first-episode schizophrenia. Arch Gen Psychiatry 51(2):124-131.

114. Brickman AM, Buchsbaum MS, Bloom R, Bokhoven P, Paul-Odouard R, Haznedar MM, Dahlman KL, Hazlett EA, Aronowitz J, Heath D and Shihabuddin L. (2004) Neuropsychological functioning in first-break, never-medicated adolescents with psychosis. J Nerv Men Dis 192(9):615-622.

115. Kravariti E, Morris RG, Rabe-Hesketh S, Murray RM, Frangou S. (2003) The Maudsley Early-Onset Schizophrenia Study: cognitive function in adolescent-onset schizophrenia. Schizophr Res 65:95-103.

116. Hoff AL, Svetina C, Maurizio AM, Crow TJ, Spokes K, DeLisi LE. (2005) Familial cognitive deficits in schizophrenia. Am J Medical Genetics Part B (Neuropsychiatric Genetics) 133B:43-

49.

117. Myles-Worsley M, Park S. (2002) Spatial working memory deficits in schizophrenia patients and their first degree relatives from Palau, Micronesia. Am J Medical Genetics (Neuropsychiatric Genetics) 114:609-615.

118. Niendam TA, Bearden CE, Rosso IM, Sanchez LE, Hadley T, Nuechterlein KH, Cannon TD. (2003) A prospective study of childhood neurocognitive functioning in schizophrenic patients and their siblings. Am J Psychiatry 160(11):2060-2062.

119. Brewer WJ, Francey SM, Wood SJ, Jackson HJ, Pantelis C, Phillips LJ, Yung AR, Anderson VA, McGorry PD. (2005) Memory impairments identified in people at ultra-high risk for psychosis who later develop first-episode psychosis. Am J Psychiatry 162(1):71-78.

120. Barch DM, Sheline YI, Csernansky JG, Snyder AZ. (2003) Working memory and prefrontal cortex dysfunction: specificity to schizophrenia compared with major depression. Biol Psychiatry 53(5):376-384.

121. Fitzgerald D, Lucas S, Redoblado MA, Winter V, Brennan J, Anderson J, Harris A. (2004) Cognitive functioning in young people with first episode psychosis: relationship to diagnosis and clinical characteristics. Australian and New Zealand J of Psychiatry 38:501-510.

122. Censits DM, Daniel Ragland J, Gur RC, Gur RE. (1997) Neuropsychological evidence supporting a neurodevelopmental model of schizophrenia: a longitudinal study. Schizophr Res 24(3):289-298.

123. Goldberg TE, Weinberger DR. (1996) Effects of neuroleptic medications on the cognition of patients with schizophrenia: a review of recent studies. J Clin Psychiatry 57(Suppl 9):62-65.

124. Kurtz MM, Ragland JD, Bilker W, Gur RC, Gur RE. (2001) Comparison of the continuous performance test with and without working memory demands in healthy controls and patients with schizophrenia. Schizophr Res 48(2-3):307-316.

125. Dickinson D, Iannone VN, Wilk CM, Gold JM. (2004) General and specific cognitive deficits in schizophrenia. Biol Psychiatry 55(8):826-833.

126. Flashman LA, Green MF. (2004) Review of cognition and brain structure in schizophrenia: profiles, longitudinal course, and effects of treatment. Psychiatr Clin North Am 27(1):1-18, vii.

127. Hill SK, Ragland JD, Gur RC, Gur RE. (2002) Neuropsychological profiles delineate distinct profiles of schizophrenia, an interaction between memory and executive function, and uneven distribution of clinical subtypes. J Clin Exp Neuropsychol 24(6):765-780.
128. Bruder GE, Wexler BE, Sage MM, Gil RB, Gorman JM. (2004) Verbal memory in schizophrenia: additional evidence of subtypes having different cognitive deficits. Schizophr Res 68(2-3):137-147.
129. Manoach D. (2003) Prefrontal cortex dysfunction during working memory performance in schizophrenia: reconciling discrepant findings. Schizophr Res 60:285-298.
130. McCarley RW, Shenton ME, O'Donnell BF, Faux SF, Kikinis R, Nestor PG, Jolesz FA. (1993) Auditory P300 abnormalities and left posterior superior temporal gyrus volume reduction in schizophrenia. Arch Gen Psychiatry 50(3):190-197.
131. Weiss A, Zalesak M, DeWitt I, Goff D, Kunkel L, Heckers S. (2004) Impaired hippocampal function during the detection of novel words in schizophrenia. Society of Biological Psychiatry 55:668-675.
132. Minzenberg MJ, Poole JH, Benton C, Vinogradov S. (2004) Association of anticholinergic load with impairment of complex attention and memory in schizophrenia. Am J Psychiatry 161:116-124.
133. Whyte MC, McIntosh AM, Johnstone EC, Lawrie SM. (2005) Declarative memory in unaffected adult relatives of patients with schizophrenia: a systematic review and meta-analysis. Schizophr Res 78(1):13- 26.
134. Barch DM, Carter CS, Braver TS, Sabb FW, MacDonald A 3rd, Noll DC, Cohen JD. (2001) Selective deficits in prefrontal cortex function in medication-naive patients with schizophrenia. Arch Gen Psychiatry 58:280-288.
135. Berman KF, Zec RF, Weinberger DR. (1986) Physiologic dysfunction of dorsolateral prefrontal cortex in schizophrenia. II. Role of neuroleptic treatment, attention, and mental effort [see comments]. Arch Gen Psychiatry 43(2):126-135.
136. Andreasen NC, O'Leary DS, Flaum M, Nopoulos P, Watkins GL, Boles Ponto LL et al. (1997) Hypofrontality in schizophrenia: Distributed dysfunctional circuits in neuroleptic-naive patients.

Lancet 349:1730- 1734.

137. Melinder MR, Barch DM. (2003) The influence of a working memory load manipulation on language production in schizophrenia. Schizophr Bull 29(3):473-485.
138. Eichenbaum H, Schoenbaum G, Young B, Bunsey M. (1996) Functional organization of the hippocampal memory system. Proc Natl Acad Sci U S A 93:13500-13507.
139. O'Reilly RC, Rudy JW. (2001) Conjunctive representations in learning and memory: principles of cortical and hippocampal function. Psychol Rev 108(2):311-345.
140. McClelland JL, McNaughton BL, O'Reilly RC. (1995) Why there are complementary learning systems in the hippocampus and neocortex: insights from the successes and failures of connectionist models of learning and memory. Psychol Rev 102(3):419-457.
141. Small SA, Schobel SA, Buxton RB, Witter MP, Barnes CA. (2011) A pathophysiological framework of hippocampal dysfunction in ageing and disease. Nature Reviews Neuroscience 12:585-601.
142. Heinrichs RW, Zakzanis KK. (1998) Neurocognitive deficit in schizophrenia: a quantitative review of the evidence. Neuropsychology 12(3):426-445.
143. Nuechterlein KH, Barch DM, Gold JM, Goldberg TE, Green MF, Heaton RK. (2004) Identification of separable cognitive factors in schizophrenia. Schizophr Res 72(1):29-39.
144. Saykin AJ, Gur RC, Gur RE, Mozley PD, Mozley LH, Resnick SM, Kester DB, Stafiniak P. (1991) Neuropsychological function in schizophrenia. Selective impairment in memory and learning. Arch Gen Psychiatry 48(7):618-624.
145. Field JR, Walker AG, Conn PJ. (2011) Targeting glutamate synapses in schizophrenia. Trends in Molecular Medicine. 19(12):689-698.
146. Bear MF. (2003) Bidirectional synaptic plasticity: from theory to reality. Philos Trans R Soc Lond B Biol Sci. 358(1432):649-655.
147. Shohamy D, Wagner AD. (2008) Integrating memories in the human brain: hippocampal-midbrain encoding of overlapping events. Neuron. 60: 378-389.
148. Aslan S, Lu H. (2010) On the sensitivity of ASL MRI in detecting regional differences in cerebral blood flow. Magn Reson Imaging. 28(7): 928-935.

149. Wu WC, Fernandez-Seara M, Detre JA, Wehrli FW, Wang J. (2007) A theoretical and experimental investigation of the tagging efficiency of pseudocontinuous arterial spin labeling. Magn Reson Med. 58(5):1020-1027.
150. Aslan S, Xu F, Wang P, Uh J, Yezhuvath U, Osch M, Lu H. (2010) Estimation of labeling efficiency in pseudo-continuous arterial spin labeling. Magn Reson Med. 63(3): 765-771.

APPENDICES

A. VASO script

HR_CBV_anal2.m

```
clear all;


studypath = '/home/guest2/work/MTL';
subjectindex = {'ND0368'};


for ii=1:length(subjectindex)
    subid = subjectindex{ii};
    vasofile = strcat(subid,'_','VASO');
    subjectpath = strcat(studypath,'/',subid);


    mkdir(strcat(subjectpath,'/',vasofile));
    cd(strcat(subjectpath,'/',vasofile));


    mat1 = 256;
    mat2 = 256;
    mat3 = 9;
    numdyn = 5;
    voxsize =  [0.78125  0.78125 4];


    outfilehead = {'pre1','pre2','pos0','pos1','pos2'};
```

```
    rawdata = read_images(strcat(subjectpath,'/',vasofile,
'.REC'),mat1,mat2,'int16',mat3*numdyn*2);  % mat3 slice x numdyn dynamic x
(modulation and phase)

    data = reshape(rawdata(:,:,1:mat3*numdyn),[mat1 mat2 mat3 numdyn]);
    SS = read_PAR(strcat(subjectpath,'/',vasofile))*[0;0;1];
    data_ss = data/SS;



    for ii = 1:5
         tmp = data_ss(:,:,:,ii);
         tmp2 = RealignImageArray(tmp,'+x-z+y');
         write_ANALYZE(tmp2,outfilehead{ii},[mat1 mat3 mat2],[voxsize(1)
voxsize(3) voxsize(2)],1,16);
    end;



    delete_if_exist('pre2.mat','pre1.mat','pos1.mat','pos2.mat');
    spm_coregistration_juh('pre2.img','pre1.img');
    spm_coregistration_juh('pre2.img','pos1.img');
    spm_coregistration_juh('pre2.img','pos2.img');

    pre2 = loadimage('pre2.img');
    rpre1 = loadimage('rpre1.img');
    rpos1 = loadimage('rpos1.img');
    rpos2 = loadimage('rpos2.img');

    CBVw_tmp = (rpos1+rpos2)/2 - (pre2+rpre1)/2;
```

```
    gap_time = 13.18;   % ms, the time between two adjacent slice
acquisitions
    acq_time = 1088+[0:8]*gap_time;
    correction_factor = (2*exp(-acq_time/1624)-exp(-6000/1624)).^(-1)

    CBVw = zeros(size(CBVw_tmp));
    for ii=1:9
        CBVw(:,ii,:) = CBVw_tmp(:,ii,:)*correction_factor(ii);
    end;

    write_ANALYZE(CBVw,'CBVw',[mat1 mat3 mat1],[voxsize(1) voxsize(3)
voxsize(2)],1,16);

end;



HR_t2_process.m

clear all;

studypath = '/home/guest2/work/MTL';

sublist = {'ND0368'};

for ii=1:length(sublist)
    array=read_images([studypath '/' sublist{ii} '/' sublist{ii}
'_highrest2.REC'],384,384,'int16',24);
    array2 = RealignImageArray(array,'+x-z+y');
```

```
    write_ANALYZE(array2,[studypath '/' sublist{ii} '/' sublist{ii}
'_VASO/HR_t2.img'],[384 24 384],[0.469 2 0.469]);
    cd(strcat(studypath,'/',sublist{ii},'/',sublist{ii},'_VASO'));
    delete_if_exist('HR_t2.mat','pre2.mat','CBVw.mat');
    spm_coregistration_juh('HR_t2.img','pre2.img','CBVw.img');
    delete_if_exist('rpre2.mat','rpre1.mat','rpos1.mat','rpos2.mat');
    spm_coregistration_juh('rpre2.img','rpre1.img');
    spm_coregistration_juh('rpre2.img','rpos1.img');
    spm_coregistration_juh('rpre2.img','rpos2.img');

end;



chop_out_small.m

Xrangelhr=209:271;
Yrangelhr=4:21;
Zrangelhr=171:223;

Xrangerhr=109:175;
Yrangerhr=4:21;
Zrangerhr=174:227;

addpath /home/guest2/work/codes
mkdir smallbox
copyfile('HR_t2.*','smallbox')
copyfile('ND*mask.*','smallbox')
copyfile('rpre2.*','smallbox')
copyfile('rCBVw.*','smallbox')
```

```
cd smallbox
delete('*.mat')

hr = loadimage('HR_t2.img');
mask = loadimage('ND0268 ROI mask.img');
regpre2 = loadimage('rpre2.img');
rCBVw = loadimage('rCBVw.img');

lhr_chop = hr(Xrangelhr,Yrangelhr,Zrangelhr);
lmask_chop = mask(Xrangelhr,Yrangelhr,Zrangelhr);
lregpre2_chop = regpre2(Xrangelhr,Yrangelhr,Zrangelhr);
lrCBVw_chop = rCBVw(Xrangelhr,Yrangelhr,Zrangelhr);

write_ANALYZE(lhr_chop,'Lhr_chop.img',[length(Xrangelhr) length(Yrangelhr)
length(Zrangelhr)],[0.469 2 0.429]);
write_ANALYZE(lmask_chop,'Lmask_chop.img',[length(Xrangelhr)  length(Yrangelhr)
length(Zrangelhr)],[0.469 2 0.429]);
write_ANALYZE(lregpre2_chop,'Lrpre2_chop.img',[length(Xrangelhr)
length(Yrangelhr) length(Zrangelhr)],[0.469 2 0.429]);
write_ANALYZE(lrCBVw_chop,'LrCBVw_chop.img',[length(Xrangelhr)
length(Yrangelhr) length(Zrangelhr)],[0.469 2 0.429]);

rhr_chop = hr(Xrangerhr,Yrangerhr,Zrangerhr);
rmask_chop = mask(Xrangerhr,Yrangerhr,Zrangerhr);
rregpre2_chop = regpre2(Xrangerhr,Yrangerhr,Zrangerhr);
rrCBVw_chop = rCBVw(Xrangerhr,Yrangerhr,Zrangerhr);

write_ANALYZE(rhr_chop,'Rhr_chop.img',[length(Xrangerhr) length(Yrangerhr)
length(Zrangerhr)],[0.469 2 0.429]);
```

```
write_ANALYZE(rmask_chop,'Rmask_chop.img',[length(Xrangerhr)  length(Yrangerhr)
length(Zrangerhr)],[0.469 2 0.429]);
write_ANALYZE(rregpre2_chop,'Rrpre2_chop.img',[length(Xrangerhr)
length(Yrangerhr) length(Zrangerhr)],[0.469 2 0.429]);
write_ANALYZE(rrCBVw_chop,'RrCBVw_chop.img',[length(Xrangerhr)
length(Yrangerhr) length(Zrangerhr)],[0.469 2 0.429]);

delete_if_exist('Lhr_chop.mat','Rhr_chop.mat','Lrpre2_chop.mat','Rrpre2_chop.
mat','LrCBVw_chop.mat','RrCBVw_chop.mat','Lpre2_chop.mat','Rpre2_chop.mat','L
CBVw_chop.mat','RCBVw_chop.mat');
spm_coregistration_juh('Lhr_chop.img','Lrpre2_chop.img','LrCBVw_chop.img');
spm_coregistration_juh('Rhr_chop.img','Rrpre2_chop.img','RrCBVw_chop.img');
```

shift_mask.m

```
% This function shift a mask image to a direction with given number of voxels
% Input:
%    inname  : input file name. it must be analyze format
%    outname : output file name
%    x : number of voxels shifted to the first dimesion direction
%    y : number of voxels shifted to the second dimesion direction
%    z : number of voxels shifted to the third dimesion direction
%    negative number is possible which means the shift to opposite direction
%
%    e.g.)  shift_mask('roi1.img','shifted_roi1.img',2,-1,3);
%
% Ouput:
%    The shifted mask matrix is the output argument
```

```
%    The shifted mask file with the output file name
%
% written by Jinsoo Uh on 2011-03-23
%

function f = shift_mask(inname,outname,x,y,z)

      [array DIM VOX SCALE TYPE OFFSET ORIGIN] = loadimage(inname);
      mat_all = size(array);
      mat1 = mat_all(1); mat2 = mat_all(2); mat3 = mat_all(3);
      outarray = zeros(size(array));

      if x>0
         array((1+x):mat1,:,:) = array(1:(mat1-x),:,:);
      else
         array(1:(mat1+x),:,:) = array((1-x):mat1,:,:);
      end;

      if y>0
         array(:,(1+y):mat2,:) = array(:,1:(mat2-y),:);
      else
         array(:,1:(mat2+y),:) = array(:,(1-y):mat2,:);
      end;

      if z>0
         array(:,:,(1+z):mat3) = array(:,:,1:(mat3-z));
      else
         array(:,:,1:(mat3+z)) = array(:,:,(1-z):mat3);
      end;
```

```
      write_analyze75_header(outname,DIM,VOX,SCALE,TYPE,OFFSET,ORIGIN,'');

      switch TYPE
        case 2
           write_binary(array,outname,'uint8');
        case 4
           write_binary(array,outname,'int16');
        case 16
           write_binary(array,outname,'float');
      end

      f = array;


% This function read a volume of image without needing to enter
% the data type and the matrix size. Those information is read
% from the header file.
%   Input:  filename ~ the file name e.g.) 'mpr.img'
%           l_scale  ~ if 1 multiply the scale in .hdr file
%                      default value is 0
%      You may use wildcards (i.e., * ) in the file name for the image files
%        of the same structure.
%      Then, the volumes of the images will be loaded to 4D matrix
%      in the sequence of the file name order.
%
%   Output : the 3D or 4D array of the image
%
```

```
function [f varargout] = loadimage(varargin)
     filename = varargin{1};
     if nargin > 1
        l_scale = varargin{2};
     else
        l_scale = 0;
     end;

     filelist = dir(filename);
     file_path=fileparts(filename);

     [DIM,VOX,SCALE,TYPE,OFFSET,ORIGIN,DESCRIP] =
read_analyze75_header(fullfile(file_path,filelist(1,1).name));
     array = zeros(DIM(1),DIM(2),DIM(3),length(filelist));


for fileindex = 1:length(filelist)

     [DIM,VOX,SCALE,TYPE,OFFSET,ORIGIN,DESCRIP] =
read_analyze75_header(fullfile(file_path,filelist(fileindex,1).name));

     fid = fopen(fullfile(file_path,filelist(fileindex,1).name),'r');
     switch TYPE
     case 2,
         dummy = fread(fid, DIM(1)*DIM(2)*DIM(3),'uint8');
     case 4,
         dummy = fread(fid, DIM(1)*DIM(2)*DIM(3),'int16');
     case 16,
         dummy = fread(fid, DIM(1)*DIM(2)*DIM(3),'float');
```

```
      case 64,
          dummy = fread(fid, DIM(1)*DIM(2)*DIM(3),'double');
      end;
      fclose(fid);

      if l_scale == 1
         array(:,:,:,fileindex) = reshape(dummy, DIM)*SCALE;
      else
         array(:,:,:,fileindex) = reshape(dummy, DIM);
      end;

end;


      f = array;
      varargout{1} = DIM;
      varargout{2} = VOX;
      varargout{3} = SCALE;
      varargout{4} = TYPE;
      varargout{5} = OFFSET;
      varargout{6} = ORIGIN;

function [DIM,VOX,SCALE,TYPE,OFFSET,ORIGIN,DESCRIP] = read_analyze75_header(P)
% reads a header
% FORMAT [DIM VOX SCALE TYPE OFFSET ORIGIN DESCRIP] = spm_hread(P);
%
% P       - filename         (e.g spm or spm.img)
% DIM     - image size       [i j k [l]] (voxels)
% VOX     - voxel size       [x y z [t]] (mm [secs])
```

```
% SCALE   - scale factor
% TYPE    - datatype (integer - see spm_type)
% OFFSET  - offset (bytes)
% ORIGIN  - origin [i j k]
% DESCRIP - description string
%_____________________________________________________________________________
%
% spm_hread reads variables into working memory from a SPM/ANALYZE
% compatible header file.  If the header does not exist global defaults
% are used.  The 'originator' field of the ANALYZE format has been
% changed to ORIGIN in the SPM version of the header.  funused1 of the
% ANALYZE format is used for SCALE
%
% see also dbh.h (ANALYZE) spm_hwrite.m and spm_type.m
%
%_____________________________________________________________________________
% @(#)spm_hread.m 2.7 99/10/29

% ensure correct suffix {.hdr}
%----------------------------------------------------------------------------
P     = deblank(P);
q     = length(P);
if q>=4 & P(q - 3) == '.'; P = P(1:(q - 4)); end
P     = [P '.hdr'];

% open header file
%----------------------------------------------------------------------------
fid   = fopen(P,'r','native');
```

```
if (fid > 0)

% read (struct) header_key
%-------------------------------------------------------------------------
fseek(fid,0,'bof');

otherendian = 0;
sizeof_hdr  = fread(fid,1,'int32');
if sizeof_hdr==1543569408, % Appears to be other-endian
      % Re-open other-endian
      fclose(fid);
      if spm_platform('bigend'),
            fid = fopen(P,'r','ieee-le');
      else,
            fid = fopen(P,'r','ieee-be');
      end;
      fseek(fid,0,'bof');
      sizeof_hdr = fread(fid,1,'int32');
      otherendian = 1;
end;

data_type   = mysetstr(fread(fid,10,'uchar'))';
db_name     = mysetstr(fread(fid,18,'uchar'))';
extents     = fread(fid,1,'int32');
session_error   = fread(fid,1,'int16');
regular     = mysetstr(fread(fid,1,'uchar'))';
hkey_un0          = mysetstr(fread(fid,1,'uchar'))';
```

```
% read (struct) image_dimension
%--------------------------------------------------------------------------
fseek(fid,40,'bof');

dim               = fread(fid,8,'int16');
vox_units         = mysetstr(fread(fid,4,'uchar'))';
cal_units         = mysetstr(fread(fid,8,'uchar'))';
unused1           = fread(fid,1,'int16');
datatype    = fread(fid,1,'int16');
bitpix            = fread(fid,1,'int16');
dim_un0           = fread(fid,1,'int16');
pixdim            = fread(fid,8,'float');
vox_offset  = fread(fid,1,'float');
funused1    = fread(fid,1,'float');
funused2    = fread(fid,1,'float');
funused3    = fread(fid,1,'float');
cal_max           = fread(fid,1,'float');
cal_min           = fread(fid,1,'float');
compressed  = fread(fid,1,'int32');
verified    = fread(fid,1,'int32');
glmax       = fread(fid,1,'int32');
glmin       = fread(fid,1,'int32');

% read (struct) data_history
%--------------------------------------------------------------------------
fseek(fid,148,'bof');

descrip           = mysetstr(fread(fid,80,'uchar'))';
```

```
aux_file    = mysetstr(fread(fid,24,'uchar'))';
orient            = fread(fid,1,'uchar');
origin            = fread(fid,5,'int16');
generated   = mysetstr(fread(fid,10,'uchar'))';
scannum           = mysetstr(fread(fid,10,'uchar'))';
patient_id  = mysetstr(fread(fid,10,'uchar'))';
exp_date    = mysetstr(fread(fid,10,'uchar'))';
exp_time    = mysetstr(fread(fid,10,'uchar'))';
hist_un0    = mysetstr(fread(fid,3,'uchar'))';
views       = fread(fid,1,'int32');
vols_added  = fread(fid,1,'int32');
start_field = fread(fid,1,'int32');
field_skip  = fread(fid,1,'int32');
omax        = fread(fid,1,'int32');
omin        = fread(fid,1,'int32');
smax        = fread(fid,1,'int32');
smin        = fread(fid,1,'int32');

fclose(fid);

if isempty(smin)
      error(['There is a problem with the header file ' P '.']);
end

% convert to SPM global variables
%-----------------------------------------------------------------------
DIM               = dim(2:4)';
VOX         = pixdim(2:4)';
SCALE       = funused1;
```

```
SCALE       = ~SCALE + SCALE;
TYPE        = datatype;
if otherendian == 1 & datatype ~= 2,
      TYPE = TYPE*256;
end;
OFFSET            = vox_offset;
ORIGIN      = origin(1:3)';
DESCRIP     = descrip(1:max(find(descrip)));

else
      global DIM VOX SCALE TYPE OFFSET ORIGIN
      DESCRIP = ['defaults'];
end
return;
%_____________________________________________________________________________

function out = mysetstr(in)
tmp = find(in == 0);
tmp = min([min(tmp) length(in)]);
out = setstr(in(1:tmp));
return;



function f =
write_analyze75_header(P,DIM,VOX,SCALE,TYPE,OFFSET,ORIGIN,DESCRIP)
% writes an ANALYZE header
% modified from spm_hwrite.m
%
```

```
% P       - filename         (e.g 'spm' or 'spm.img')
% DIM     - image size       [i j k [l]] (voxels)
% VOX     - voxel size       [x y z [t]] (mm [sec])
% SCALE   - scale factor
% TYPE    - datatype (integer - see spm_type)
% OFFSET  - offset (bytes)
% ORIGIN  - [i j k] of origin  (default = [0 0 0])
% DESCRIP - description string (default = 'spm compatible')
%


P               = P(P ~= ' ');
q           = length(P);
if q>=4 & P(q - 3) == '.', P = P(1:(q - 4)); end;
P                = [P '.hdr'];


fid             = fopen(P,'w','native');
%fid             = fopen(P,'w','ieee-le');
%fid             = fopen(P,'w','ieee-be');


%--------------------------------------------------------------------------
data_type   = ['dsr      ' 0];


P                = [P '                  '];
db_name          = [P(1:17) 0];


% set header variables
%--------------------------------------------------------------------------
DIM         = DIM(:)'; if size(DIM,2) < 4; DIM = [DIM 1]; end
VOX         = VOX(:)'; if size(VOX,2) < 4; VOX = [VOX 0]; end
```

```
dim         = [4 DIM(1:4) 0 0 0];
pixdim            = [0 VOX(1:4) 0 0 0];
vox_offset      = OFFSET;
funused1    = SCALE;
glmax       = 1;
glmin       = 0;
bitpix            = 0;
descrip         = zeros(1,80);
aux_file        = ['none                    ' 0];
origin          = [0 0 0 0 0];

%--------------------------------------------------------------------------
if TYPE == 1;   bitpix = 1;  glmax = 1;        glmin = 0;   end
if TYPE == 2;   bitpix = 8;  glmax = 255;      glmin = 0;   end
if TYPE == 4;   bitpix = 16; glmax = 32767;    glmin = 0;   end
if TYPE == 8;   bitpix = 32; glmax = (2^31-1); glmin = 0;   end
if TYPE == 16;  bitpix = 32; glmax = 1;        glmin = 0;   end
if TYPE == 64;  bitpix = 64; glmax = 1;        glmin = 0;   end

%--------------------------------------------------------------------------
if nargin >= 7; origin = [ORIGIN(:)' 0 0];  end
if nargin <  8; DESCRIP = 'spm compatible'; end

d           = 1:min([length(DESCRIP) 79]);
descrip(d)  = DESCRIP(d);

fseek(fid,0,'bof');

% write (struct) header_key
```

```
%---------------------------------------------------------------------------
fwrite(fid,348,         'int32');
fwrite(fid,data_type,   'char' );
fwrite(fid,db_name,     'char' );
fwrite(fid,0,           'int32');
fwrite(fid,0,           'int16');
fwrite(fid,'r',         'char' );
fwrite(fid,'0',         'char' );

% write (struct) image_dimension
%---------------------------------------------------------------------------
fseek(fid,40,'bof');

fwrite(fid,dim,         'int16');
fwrite(fid,'mm',  'char' );
fwrite(fid,0,           'char' );
fwrite(fid,0,           'char' );

fwrite(fid,zeros(1,8),  'char' );
fwrite(fid,0,           'int16');
fwrite(fid,TYPE,  'int16');
fwrite(fid,bitpix,      'int16');
fwrite(fid,0,           'int16');
fwrite(fid,pixdim,      'float');
fwrite(fid,vox_offset,  'float');
fwrite(fid,funused1,    'float');
fwrite(fid,0,           'float');
fwrite(fid,0,           'float');
fwrite(fid,0,           'float');
```

```
fwrite(fid,0,           'float');
fwrite(fid,0,           'int32');
fwrite(fid,0,           'int32');
fwrite(fid,glmax, 'int32');
fwrite(fid,glmin, 'int32');

% write (struct) image_dimension
%--------------------------------------------------------------------------
fwrite(fid,descrip,     'char');
fwrite(fid,aux_file,    'char');
fwrite(fid,0,           'char');
fwrite(fid,origin,      'int16');

if fwrite(fid,zeros(1,85), 'char')~=85
      fclose(fid);
end

fclose(fid);
```

scaledROI_smallbox_corr_thalamus.m

```
 studypath = '/home/guest2/work/MTL';

subjectindex = {'ND0268'};

scaledHippROI = zeros(length(subjectindex),8);
HippROIvoxelNum = zeros(length(subjectindex),8);
combinedHippROI = zeros(length(subjectindex),6);
```

```
combinedHippROIvoxelNum = zeros(length(subjectindex),6);


for ii=1:length(subjectindex)
    subid = subjectindex{ii};
    vasofile = strcat(subid,'_','VASO');
    subjectpath = strcat(studypath,'/',subid);
    cd(strcat(subjectpath,'/',vasofile,'/smallbox'));
    maskname = strcat(subid, ' ROI mask.img');
    hipp_mask = loadimage(maskname);
    RHippMask = loadimage('Rmask_chop_shift.img');
    LHippMask = loadimage('Lmask_chop_shift.img');
    rCBVw = loadimage('rCBVw.img');
    rRrCBVw_chop = loadimage('rRrCBVw_chop.img');
    rLrCBVw_chop = loadimage('rLrCBVw_chop.img');

    ss_mask = loadimage('thalamus.img');
    rCBVw = loadimage('rCBVw.img');
    scalingfactor = mean(rCBVw(find((ss_mask==100) & (~isnan(ss_mask)))))
    factor = mean(rCBVw(find((ss_mask==100) & (~isnan(ss_mask)))));


    thresh = 1000;
    scalingfactor = mean(RrCBVw_chop( (find( (RHippMask==1) &
(~isnan(RrCBVw_chop)) & (RrCBVw_chop>0) & (RrCBVw_chop<thresh)))))

    scaledHippROI(ii,1)=mean(rRrCBVw_chop( (find( (RHippMask==1) &
(~isnan(rRrCBVw_chop)) & (rRrCBVw_chop>0) &
(rRrCBVw_chop<thresh)))))/scalingfactor*100;
```

```
    HippROIvoxelNum(ii,1)=numel(rRrCBVw_chop( (find( (RHippMask==1) &
(~isnan(rRrCBVw_chop)) & (rRrCBVw_chop>0) & (rRrCBVw_chop<thresh)))));
    scaledHippROI(ii,2)=mean(rRrCBVw_chop( (find( (RHippMask==2) &
(~isnan(rRrCBVw_chop)) & (rRrCBVw_chop>0) &
(rRrCBVw_chop<thresh)))))/scalingfactor*100;
    HippROIvoxelNum(ii,2)=numel(rRrCBVw_chop( (find( (RHippMask==2) &
(~isnan(rRrCBVw_chop)) & (rRrCBVw_chop>0) & (rRrCBVw_chop<thresh)))));
    scaledHippROI(ii,3)=mean(rRrCBVw_chop( (find( (RHippMask==3) &
(~isnan(rRrCBVw_chop)) & (rRrCBVw_chop>0) &
(rRrCBVw_chop<thresh)))))/scalingfactor*100;
    HippROIvoxelNum(ii,3)=numel(rRrCBVw_chop( (find( (RHippMask==3) &
(~isnan(rRrCBVw_chop)) & (rRrCBVw_chop>0) & (rRrCBVw_chop<thresh)))));
    scaledHippROI(ii,4)=mean(rRrCBVw_chop( (find( (RHippMask==4) &
(~isnan(rRrCBVw_chop)) & (rRrCBVw_chop>0) &
(rRrCBVw_chop<thresh)))))/scalingfactor*100;
    HippROIvoxelNum(ii,4)=numel(rRrCBVw_chop( (find( (RHippMask==4) &
(~isnan(rRrCBVw_chop)) & (rRrCBVw_chop>0) & (rRrCBVw_chop<thresh)))));
    scaledHippROI(ii,5)=mean(rLrCBVw_chop( (find( (LHippMask==5) &
(~isnan(rLrCBVw_chop)) & (rLrCBVw_chop>0) &
(rLrCBVw_chop<thresh)))))/scalingfactor*100;
    HippROIvoxelNum(ii,5)=numel(rLrCBVw_chop( (find( (LHippMask==5) &
(~isnan(rLrCBVw_chop)) & (rLrCBVw_chop>0) & (rLrCBVw_chop<thresh)))));
    scaledHippROI(ii,6)=mean(rLrCBVw_chop( (find( (LHippMask==6) &
(~isnan(rLrCBVw_chop)) & (rLrCBVw_chop>0) &
(rLrCBVw_chop<thresh)))))/scalingfactor*100;
    HippROIvoxelNum(ii,6)=numel(rLrCBVw_chop( (find( (LHippMask==6) &
(~isnan(rLrCBVw_chop)) & (rLrCBVw_chop>0) & (rLrCBVw_chop<thresh)))));
```

```
    scaledHippROI(ii,7)=mean(rLrCBVw_chop( (find( (LHippMask==7) &
(~isnan(rLrCBVw_chop)) & (rLrCBVw_chop>0) &
(rLrCBVw_chop<thresh)))))/scalingfactor*100;
    HippROIvoxelNum(ii,7)=numel(rLrCBVw_chop( (find( (LHippMask==7) &
(~isnan(rLrCBVw_chop)) & (rLrCBVw_chop>0) & (rLrCBVw_chop<thresh))));
    scaledHippROI(ii,8)=mean(rLrCBVw_chop( (find( (LHippMask==8) &
(~isnan(rLrCBVw_chop)) & (rLrCBVw_chop>0) &
(rLrCBVw_chop<thresh)))))/scalingfactor*100;
    HippROIvoxelNum(ii,8)=numel(rLrCBVw_chop( (find( (LHippMask==8) &
(~isnan(rLrCBVw_chop)) & (rLrCBVw_chop>0) & (rLrCBVw_chop<thresh))));

    combinedHippROI(ii,1)=mean(rRrCBVw_chop( (find( ((RHippMask==3) |
(RHippMask==4)) & (~isnan(rRrCBVw_chop)) & (rRrCBVw_chop>0) &
(rRrCBVw_chop<thresh)))))/scalingfactor*100;
    combinedHippROIvoxelNum(ii,1)=numel(rRrCBVw_chop( (find( ((RHippMask==3)
| (RHippMask==4)) & (~isnan(rRrCBVw_chop)) & (rRrCBVw_chop>0) &
(rRrCBVw_chop<thresh))));
    combinedHippROI(ii,2)=mean(rRrCBVw_chop( (find( ((RHippMask==2) |
(RHippMask==3) | (RHippMask==4)) & (~isnan(rRrCBVw_chop)) & (rRrCBVw_chop>0)
& (rRrCBVw_chop<thresh)))))/scalingfactor*100;
    combinedHippROIvoxelNum(ii,2)=numel(rRrCBVw_chop( (find( ((RHippMask==2)
| (RHippMask==3) | (RHippMask==4)) & (~isnan(rRrCBVw_chop)) & (rRrCBVw_chop>0)
& (rRrCBVw_chop<thresh))));
    combinedHippROI(ii,3)=mean(rRrCBVw_chop( (find( ((RHippMask==1) |
(RHippMask==2) | (RHippMask==3) | (RHippMask==4)) & (~isnan(rRrCBVw_chop)) &
(rRrCBVw_chop>0) & (rRrCBVw_chop<thresh)))))/scalingfactor*100;
    combinedHippROIvoxelNum(ii,3)=numel(rRrCBVw_chop( (find( ((RHippMask==1)
| (RHippMask==2) | (RHippMask==3) | (RHippMask==4)) & (~isnan(rRrCBVw_chop))
& (rRrCBVw_chop>0) & (rRrCBVw_chop<thresh))));
```

```
    combinedHippROI(ii,4)=mean(rLrCBVw_chop( (find( ((LHippMask==7) |
(LHippMask==8)) & (~isnan(rLrCBVw_chop)) & (rLrCBVw_chop>0) &
(rLrCBVw_chop<thresh)))))/scalingfactor*100;
    combinedHippROIvoxelNum(ii,4)=numel(rLrCBVw_chop( (find( ((LHippMask==7)
| (LHippMask==8)) & (~isnan(rLrCBVw_chop)) & (rLrCBVw_chop>0) &
(rLrCBVw_chop<thresh)))));
    combinedHippROI(ii,5)=mean(rLrCBVw_chop( (find( ((LHippMask==6) |
(LHippMask==7) | (LHippMask==8)) & (~isnan(rLrCBVw_chop)) & (rLrCBVw_chop>0)
& (rLrCBVw_chop<thresh)))))/scalingfactor*100;
    combinedHippROIvoxelNum(ii,5)=numel(rLrCBVw_chop( (find( ((LHippMask==6)
| (LHippMask==7) | (LHippMask==8)) & (~isnan(rLrCBVw_chop)) & (rLrCBVw_chop>0)
& (rLrCBVw_chop<thresh)))));
    combinedHippROI(ii,6)=mean(rLrCBVw_chop( (find( ((LHippMask==5) |
(LHippMask==6) | (LHippMask==7) | (LHippMask==8)) & (~isnan(rLrCBVw_chop)) &
(rLrCBVw_chop>0) & (rLrCBVw_chop<thresh)))))/scalingfactor*100;
    combinedHippROIvoxelNum(ii,6)=numel(rLrCBVw_chop( (find( ((LHippMask==5)
| (LHippMask==6) | (LHippMask==7) | (LHippMask==8)) & (~isnan(rLrCBVw_chop))
& (rLrCBVw_chop>0) & (rLrCBVw_chop<thresh)))));

end;

R_DG_NV_SVon_SVoff =[mean(scaledHippROI(1:24,1)) mean(scaledHippROI(25:46,1))
mean(scaledHippROI(47:61,1))]
R_Subi_NV_SVon_SVoff =[mean(scaledHippROI(1:24,2))
mean(scaledHippROI(25:46,2)) mean(scaledHippROI(47:61,2))]
R_CA3_NV_SVon_SVoff =[mean(scaledHippROI(1:24,3)) mean(scaledHippROI(25:46,3))
mean(scaledHippROI(47:61,3))]
R_CA1_NV_SVon_SVoff =[mean(scaledHippROI(1:24,4)) mean(scaledHippROI(25:46,4))
mean(scaledHippROI(47:61,4))]
```

```
L_DG_NV_SVon_SVoff =[mean(scaledHippROI(1:24,5)) mean(scaledHippROI(25:46,5))
mean(scaledHippROI(47:61,5))]
L_Subi_NV_SVon_SVoff =[mean(scaledHippROI(1:24,6))
mean(scaledHippROI(25:46,6)) mean(scaledHippROI(47:61,6))]
L_CA3_NV_SVon_SVoff =[mean(scaledHippROI(1:24,7)) mean(scaledHippROI(25:46,7))
mean(scaledHippROI(47:61,7))]
L_CA1_NV_SVon_SVoff =[mean(scaledHippROI(1:24,8)) mean(scaledHippROI(25:46,8))
mean(scaledHippROI(47:61,8))]
scaledHippROI
HippROIvoxelNum

R_CA3CA1_NC_SZon_SZoff = [mean(combinedHippROI(1:24,1))
mean(combinedHippROI(25:46,1)) mean(combinedHippROI(47:61,1))]
R_SubiCA3CA1_NC_SZon_SZoff = [mean(combinedHippROI(1:24,2))
mean(combinedHippROI(25:46,2)) mean(combinedHippROI(47:61,2))]
R_DGSubiCA3CA1_NC_SZon_SZoff = [mean(combinedHippROI(1:24,3))
mean(combinedHippROI(25:46,3)) mean(combinedHippROI(47:61,3))]
L_CA3CA1_NC_SZon_SZoff = [mean(combinedHippROI(1:24,4))
mean(combinedHippROI(25:46,4)) mean(combinedHippROI(47:61,4))]
L_SubiCA3CA1_NC_SZon_SZoff = [mean(combinedHippROI(1:24,5))
mean(combinedHippROI(25:46,5)) mean(combinedHippROI(47:61,5))]
L_DGSubiCA3CA1_NC_SZon_SZoff = [mean(combinedHippROI(1:24,6))
mean(combinedHippROI(25:46,6)) mean(combinedHippROI(47:61,6))]
combinedHippROI
combinedHippROIvoxelNum
```

B. pCASL script

```
pro_pcasl_realign_calcCBF_multiplesubjects.m

studypath='/home/guest2/work/MTL/PCASL';


subjectindex={'ND0254'};
% Parameters that may need to be changed
dynnum=60;
rownum=80;
columnnum=80;
slicenum=27;
resolution=[3,3,5];


% Other parameters that don't need to be changed.
labldur=1650;  % ms, labeling duration
PDL = 1525;  % post labeling delay, ms.
Sind = 14;  % slice number that contains thalamus; to be used for M0
quantificaation.
TE = 13.79;  % ms
SRtime=3704;  % ms
w=35;  % ms, acquisition delay between adjacent slices
T1tissue=933.5 ;% ms, tissue T1 = (Gray T1 + White T1)/2,, from Lu 2005
T1a = 1278.7;% ms T1  = (blood T1+ tissue T1)/2, from Lu 2004,2005
lambda = 0.9; % unit: ml/g;
alpha = 0.86;  % Sina et al, 2010


for mysubject=1:length(subjectindex)
    temp1=subjectindex{mysubject}
    filename=strcat('PCASL');
```

```
    subjectpath=strcat(studypath,'/',temp1);


%realign images
warning off;
    img_all=zeros(rownum,columnnum,slicenum,dynnum);
    target=strcat(subjectpath,'/',filename,'/',filename,'-001-001.img');
    for count=1:dynnum
        if count<10
            a=strcat('00',int2str(count));
        elseif count<100
            a=strcat('0',int2str(count));
        else
            a=int2str(count);
        end
        source=strcat(subjectpath,'/',filename,'/',filename,'-',a,'-001.img');
        other=source;
        spm_defaults;
        defs=defaults.realign;
        FlagsC = struct('quality',defs.estimate.quality,'fwhm',5,'rtm',0);
        spm_realign([target;source],FlagsC);
        FlagsR = struct('interp',defs.write.interp,...
        'wrap',defs.write.wrap,...
        'mask',defs.write.mask,...
        'which',2,'mean',1);
        FlagsR.which = 2; FlagsR.mean = 1;
        spm_reslice([target;source],FlagsR);

thisimg=read_images_vms(strcat(subjectpath,'/',filename,'/r',filename,'-
',a,'-001.img'), rownum, columnnum, 'int16',slicenum);
```

```
        img_all(:,:,:,count)=thisimg(:,:,:);
    end

% calculate difference map
    label = mean(img_all(:,:,:,1:2:dynnum),4);
    control = mean(img_all(:,:,:,2:2:dynnum),4);
    diff = control - label;

% find M0 for absolute CBF calculation
% draw an ROI to cover all brain voxels
    handle = figure();
    i=1;
    roiall=[];
    done='n';
    while(done ~= 'y')
    img = reshape(control(:,:,Sind), rownum, columnnum);
    imshow(img, [min(img(:)), max(img(:))]);
    colormap(gray);
    BW=roipoly;
    roiplane=img.*BW;
    roiall=[roiall; roiplane(find(roiplane>0))];
    done = input('Finished? (y/n)','s');
    end
    close all;
% calculate M0
    M0=mean(roiall)/(1-exp(-SRtime/T1tissue));
    save([subjectpath filesep filename filesep 'M0.txt'], 'M0','-ascii');

% calculate CBF
```

```
    f=zeros(size(diff));
    for kk=1:size(f,3)
% correction for the different delay time for different slice
    sPDL = PDL + (kk-1)*w;
% calculate absolute CBF from ASL signal
    f(:,:,kk) = diff(:,:,kk)/M0*lambda/(2*alpha*T1a*(exp(-sPDL/T1a)-exp(-
(sPDL+labldur)/T1a)))*60*100*1000;
end;

% Thresholding CBF weighted image to remove the dark spots and ultra
% bright spots in CBF weighted images in the raw data space
fthre=f;
fthre(f<0)=0;
fthre(f>200)=200;

% save CBF maps
write_ANALYZE(f,strcat(subjectpath,'/',filename,'/','aCBFw'),[rownum,
columnnum, slicenum],resolution,1,16);
write_ANALYZE(fthre,strcat(subjectpath,'/',filename,'/','tCBFw'),[rownum,
columnnum, slicenum],resolution,1,16);

end
```

C. AE ROI analysis script

Percent_signal_change.m

```
clear all;

addpath /r/fmri/lib64/matlab/2007a/toolbox/spm5/toolbox/marsbar;
addpath /r/fmri/lib64/matlab/2007a/toolbox/spm2/toolbox/marsbar;
studypath = '/home/ttest/MTL';

HippoL = '/home/ttest/MTL/AE_ROI_analysis/hippocampus_L_roi.mat';
HippoR = '/home/ttest/MTL/AE_ROI_analysis/hippocampus_R_roi.mat';
Midbrain = '/home/ttest/MTL/AE_ROI_analysis/midbrain_roi.mat';

subjectindex = {'ND-0360'};

for ii = 1:length(subjectindex)
    subid = subjectindex{ii};
    subjectpath = strcat(studypath,'/',subid);
    spm_name = strcat(subjectpath,'/AE/work/SPM.mat');

% Make marsbar design object
    SPM = load(spm_name);
    D = mardo(SPM);

    % Make marsbar ROI object
    HippoLROI = maroi(HippoL);
    HippoRROI = maroi(HippoR);
    MidbrainROI = maroi(Midbrain);
```

```
% Fetch data into marsbar data object
    HippoLROI = get_marsy(HippoLROI, D, 'mean');
    HippoRROI = get_marsy(HippoRROI, D, 'mean');
    MidbrainROI = get_marsy(MidbrainROI, D, 'mean');

% Get contrasts from original design
    Con = get_contrasts(D);

% Estimate design on ROI data
    HippoLE = estimate(D, HippoLROI);
    HippoRE = estimate(D, HippoRROI);
    MidbrainE = estimate(D, MidbrainROI);

% Put contrasts from original design back into design object
    HippoLE = set_contrasts(HippoLE, Con);
    HippoRE = set_contrasts(HippoRE, Con);
    MidbrainE = set_contrasts(MidbrainE, Con);

% Get design betas
    HippoLb = betas(HippoLE);
    HippoRb = betas(HippoRE);
    Midbrainb = betas(MidbrainE);

% Get stats and stuff for all contrasts into statistics structure
    HippoLmarsS = compute_contrasts(HippoLE, 1:length(Con));
    HippoRmarsS = compute_contrasts(HippoRE, 1:length(Con));
    MidbrainmarsS = compute_contrasts(MidbrainE, 1:length(Con));
```

```
% Extract all the FIR timecourses from design and return pct signal estimates
    ROIindex = {HippoLE,HippoRE,MidbrainE};
    for jj = 1:length(ROIindex)
        E = ROIindex{jj};

% One session
% Get definitions of all events in model
        [e_specs, e_names] = event_specs(E);
        n_events = size(e_specs, 2);

% Bin size in seconds for FIR
        bin_size = tr(E);

% Length of FIR in seconds
        fir_length = 24;

% Number of FIR time bins to cover length of FIR
        bin_no = fir_length / bin_size;

% Options - here 'single' FIR model, return estimated percent signal change
        opts = struct('single', 1, 'percent', 1);

        dur = 0;
% One session
% Return time courses for all events in fir_tc matrix
        for e_s = 1:n_events
            fir_tc(:, e_s) = event_fitted_fir(E, e_specs(:, e_s), bin_size,
bin_no, opts);
            pct_ev(e_s) = event_signal(E, e_specs(:,e_s), dur);
```

```
        end


        pct_ev;
        auc = sum(fir_tc(2:6,:));
        mean([pct_ev(7) pct_ev(8) pct_ev(9) pct_ev(11) pct_ev(12) pct_ev(13)])
% No Run4
%        mean([pct_ev(7) pct_ev(8) pct_ev(9)])
% No Run1 or Run2
%        mean([pct_ev(4) pct_ev(5) pct_ev(6) pct_ev(8) pct_ev(9) pct_ev(10)])
% No Run1 and Run2
%        mean([pct_ev(1) pct_ev(2) pct_ev(3) pct_ev(5) pct_ev(6) pct_ev(7)])
        mean([auc(7) auc(8) auc(9) auc(11) auc(12) auc(13)])
% No Run4
%        mean([auc(7) auc(8) auc(9)])
% No Run1 or Run2
%        mean([auc(4) auc(5) auc(6) auc(8) auc(9) auc(10)])
% No Run1 and Run2
%        mean([auc(1) auc(2) auc(3) auc(5) auc(6) auc(7)])
        mean([pct_ev(10) pct_ev(14)])
% No Run4
%        mean([pct_ev(10)])
% No Run1 or Run2
%        mean([pct_ev(7) pct_ev(11)])
% No Run1 and Run2
%        mean([pct_ev(4) pct_ev(8)])
        mean([auc(10) auc(14)])
% No Run4
%        mean([auc(10)])
% No Run1 or Run2
```

```
%        mean([auc(7) auc(11)])
% No Run1 and Run2
%        mean([auc(4) auc(8)])
    end
end
```